

Transition between [R]- and [S]-Stereoisomers without Bond Breaking

by

shampa.santra , Komal Yadav, Rojisha V. C., Tanashree Jaganade, Prathyusha V, Swetha Bikkina,
Upakarasamy Lourderaj, U Deva Priyakumar

in

Physical Chemistry Chemical Physics

Report No: IIIT/TR/2020/-1



Centre for Computational Natural Sciences and Bioinformatics
International Institute of Information Technology
Hyderabad - 500 032, INDIA
June 2020

Transition between [R]- and [S]-Stereoisomers without Bond Breaking

Shampa Raghunathan, Komal Yadav, V. C. Rojisha, Tanashree Jaganade, V. Prathyusha, Swetha Bikkina, Upakarasamy Lourderaj, U. Deva Priyakumar

Submitted date: 30/05/2020 • Posted date: 01/06/2020

Licence: CC BY-NC-ND 4.0

Citation information: Raghunathan, Shampa; Yadav, Komal; Rojisha, V. C.; Jaganade, Tanashree; Prathyusha, V.; Bikkina, Swetha; et al. (2019): Transition between [R]- and [S]-Stereoisomers without Bond Breaking. ChemRxiv. Preprint. <https://doi.org/10.26434/chemrxiv.8010311.v2>

We for the first time shown that transition between (R) and (S) stereoisomers via a planar transition state or an intermediate structure without having to break a bond is possible. Rigorous theoretical calculations have been used to study this novel phenomenon and to characterize the energetic, structure, dynamic and kinetic properties.

File list (3)

pccp_final.pdf (5.67 MiB)

[view on ChemRxiv](#) • [download file](#)

pccp_si.pdf (7.67 MiB)

[view on ChemRxiv](#) • [download file](#)

out5a-1.mp4 (7.07 MiB)

[view on ChemRxiv](#) • [download file](#)

Cite this: DOI: 00.0000/xxxxxxxxxx

Transition between [R]- and [S]-Stereoisomers without Bond Breaking[†]

Shampa Raghunathan,^{a‡} Komal Yadav,^{b‡} V. C. Rojisha,^a Tanashree Jaganade,^a V. Prathyusha,^a Swetha Bikkina,^a Upakarasamy Lourderaj,^{*b} and U. Deva Priyakumar^{*a}Received Date
Accepted Date

DOI: 00.0000/xxxxxxxxxx

The fifty-year proposal of nondissociative racemization reaction of a tetracoordinated tetrahedral center from one enantiomer to another via a planar transition state by Hoffmann and coworkers has been explored by many research groups during the past five decades. A number of stable molecules with planar tetracoordinate and higher-coordinate centers have been designed and experimentally realized; however, there has not been a single example of molecular system that can possibly undergo such racemization. Here we show examples of molecular species that undergo inversion of stereochemistry around tetrahedral centers (Si, Al⁻ and P⁺) either via a planar transition state or an intermediate state using quantum mechanical, *ab initio* quasi-classical dynamics calculations, and Born-Oppenheimer molecular dynamics (BOMD) simulations. This work is expected to provide potential leads for future studies on this fundamental phenomenon in chemistry.

1 Introduction

Preference of tetrahedral geometry by tetracoordinate carbon centers was reported independently by van't Hoff¹ and Le Bel² in 1874. This cornerstone principle in chemistry is so general that no exception to this rule was found for about a century. Wynberg and coworkers³ in 1965 found no optical activity for chiral butylethylhexylpropylmethane, but ruled out the possibility of interconversion between two enantiomers. Inspired by this experiment, Monkhorst⁴ examined pathways for interconversion between enantiomers without breaking any bond (termed as stereomutation) using SCF calculations and concluded that it "is in fact impossible" and that it "would require at least 2-5 times the carbon-carbon bond energy", indicating that bond breaking is imminent for the process of racemization. Hoffmann and coworkers⁵ investigated the electronic structure of planar methane to explore means by which the planar tetracoordinate geometry could

be stabilized such that it can act as a transition state for viable stereomutation. Though a stable molecule was not identified, they proposed elegant strategies by which a planar tetracoordinate carbon (ptC) could be stabilized. Following this, Collins et al.⁶ showed the planar forms of Li-substituted cyclopropane and cyclopropene to be more stable than their tetrahedral counterparts. A year later, the first compound with a ptC center was synthesized by Cotton and Millar.⁷

Next several years witnessed characterization of numerous molecular models with a planar tetracoordinate center⁸⁻¹³ based on the methane model.¹⁴ The thermodynamic stabilities of these molecules were attained either by electronic or mechanical stabilization of the planar center. The central atom of the planar tetracoordinate molecule holds a lone pair of electrons and consequently the in-plane σ -bonds are electron deficient. Therefore, electronic stabilization is accomplished by having π -acceptors and σ -donors as substituents.⁵ On the other hand, in the mechanical approach, a central planar tetracoordinated carbon atom is structurally constrained by forming a cage around it.¹⁵⁻²¹ Wong and Radom²² showed that the planar form of methane dication is a minimum but does not exhibit a square shape and about a decade later Wang and Schleyer²³ found similar planar form of methane dication that lacks the lone pair in the central atom to be a minimum on its potential energy surface (PES) and proposed this to be an alternative model based on which a large number of species have been designed. Recently, two hydrogenated ptC species, CA_4H and CA_4H^- were identified based on a photoelectron spectroscopic and quantum chemical study.²⁴

^a Center for Computational Natural Sciences and Bioinformatics International Institute of Information Technology, Hyderabad 500 032, India. E-mail: deva@iiit.ac.in

^b School of Chemical Sciences, National Institute of Science Education and Research, Bhubaneswar, HBNI, P.O. Jatani, Khordha, 752050, India. E-mail: u.lourderaj@niser.ac.in

[†] Electronic Supplementary Information (ESI) available: [Details on EDA-NOCV analysis. Energetics, and structures (bond lengths and angles) of each intermediate, and transition state, additionally the CASSCF energies. Reactive *ab initio* classical trajectories for Si, Al⁻, P⁺ and chiral-Si systems. MSM conformational clustering, and computing details of lifetimes of closed, and open states. Traversing of the Si-system on the potential energy surface presented in a multimedia file]. See DOI: 00.0000/00000000.

[‡] Authors contributed equally to this work.

For nearly fifty years, significant progress has been made in terms of theoretical design and experimental realization of chemical moieties with planar tetracoordinate carbon or isoelectronic counterparts such as B^- , N^+ , Si, Al^- and P^+ .^{25–34} Several molecules consisting of planar hypercoordinate centers have also been reported.^{35–42}

Hoffmann and coworkers⁵ in their seminal paper anticipated that realizing a stable planar tetracoordinate center would be “too much to hope” than to design one that “could serve as a thermally accessible transition state for a classical racemization experiment”. The studies that followed have shown the reverse to be true where many stable planar structures have been found, but no example that met the original objective of achieving stereomutation of a tetrahedral center via a planar transition state has been identified. In cases where a molecule with a planar center is a minimum on its PES, the corresponding tetrahedral form is (a) structurally not plausible, (b) a higher order saddle point, or (c) significantly high in energy. In this study, we report the first ever examples of molecular models that undergo classical racemization via a planar transition state or a planar intermediate state involving Si, Al^- and P^+ without bond dissociation. We also identify a system for which four different stereoisomers are possible for a single chiral center that can interconvert among themselves. We have used high-level *ab initio* calculations, *ab initio* quasi-classical trajectory simulations and density functional theory (DFT) based Born-Oppenheimer molecular dynamics (BOMD) simulations to rigorously characterize these molecules and to calculate thermodynamic and kinetic properties for the interconversion pathways.

2 Methodology

2.1 Quantum mechanical calculations

Geometry optimizations and frequency calculations were performed at the MP2 level and single point energy calculations were done at the CCSD(T) level using the cc-pVTZ⁴³ basis set employing the Gaussian 09⁴⁴ program package. Potential energy surfaces were generated at the MP2/cc-pVTZ level with respect one or two geometric parameters as mentioned in the main text. Quantitative agreement was obtained with the two levels of theory and hence for uniformity, data from the MP2/cc-pVTZ level is presented unless otherwise specified. To ascertain the importance of static correlation in the isomerization pathways, CASSCF calculations were performed using stationary point geometries obtained at the MP2/cc-pVTZ level of theory for the $X = Si$ and P^+ systems. Two active spaces, (8,8) and (14,14) were used in the calculations. In addition, CASPT2/cc-pVTZ calculations were also performed using (8,8) active space to include dynamic correlation effects.

2.2 *Ab initio* classical trajectory simulations

Ab initio quasi-classical trajectory simulations⁴⁵ were carried out using VENUS/NWChem programs^{46,47} at the MP2/cc-pVTZ level of theory. A total of 50 trajectories were initiated from the reactant region using microcanonical normal mode sampling procedure.⁴⁸ From the classical minimum of the reactants, an ex-

cess energy of 40.79, 40.92 and 42.95 kcal/mol for $X = Si$, Al^- , and P^+ systems respectively were given. These energies approximately correspond to the sum of average vibrational, rotational, and translational energies of the molecule at 300 K assuming a Boltzmann distribution. The trajectories were initiated for a total time of 2 ps each using velocity-Verlet⁴⁹ algorithm, with *ab initio* forces computed at the MP2/cc-pVTZ level of theory.

2.3 Born-Oppenheimer molecular dynamics

We have performed Born-Oppenheimer molecular dynamics (BOMD) simulations for planar $p-Al^-$, $p-Si$ and $p-P^+$ using the Car-Parrinello MD (CPMD)⁵⁰ package which unifies density functional theory (DFT) and MD. MP2/cc-pVTZ optimized geometries were taken as initial structures for BOMD simulations. They were then optimized and equilibrated. In the BOMD simulations of the systems reported here, Goedecker⁵¹ type pseudopotentials (in the Kleinman-Bylander⁵² form) have been used for all atoms and the valence electronic orbitals were expanded in plane waves with the maximum kinetic energy cutoff of 85 Rydberg. BLYP^{53,54} gradient-corrected exchange-correlation functional was used. The equations of motion for ions were integrated using a molecular dynamics time step of 25 a.u. (≈ 0.6 fs). The simulation length was 400 ps. The equilibrium temperature (300 K) was controlled with the Nose-Hoover chain thermostats.

3 Results and discussion

Motivated by the successful design of the ptC with a central carbon atom of molecule $C(C_2)((CH_2)_2)$ – a spiroconjugation of two 3-membered rings⁵⁵, we have devised novel stabilized systems by replacing the central C atom by its valence isoelectronic species from the second row of the periodic table, $X = Si$, Al^- and P^+ . When the central spiro carbon atom is replaced by a second row atom/ion, presumed to possess unoccupied *d* orbitals that are relatively low in energy, further stabilization is expected to occur.⁵⁶ Energy minimization of the tetrahedral (**t-X**) and planar (**p-X**) forms of the structures (Figure 1a) reveals that all the **t-X** structures lie about 3.5–5 kcal/mol lower in energy than the corresponding **p-X** structures. Frequency calculations characterize the **t-X** structures to be minima in all three cases. The geometry optimizations and frequency calculations were done using the MP2/cc-pVTZ level of theory and the energies were found to be in good agreement with the coupled cluster CCSD(T) method (See Figure S1 for optimized geometries, and Table S2 for energies in the supporting information). All the discussions on the QM and dynamics calculations are based on the results obtained using the MP2/cc-pVTZ method unless noted. The **p-X**, when $X = Si$ and Al^- , are found to be transition states, where the normal mode of the imaginary frequency corresponds to an asymmetric rotation of the two three-membered rings about the central atom X. Intrinsic reaction coordinate (IRC) calculations following these normal modes lead to the tetrahedral forms along both sides of the maximum. In other words, planar forms ($X = Si$ and Al^-) are characterized as transition states for the stereomutation process about central atoms – in this case, the transition between two identical tetrahedral forms. Interestingly for $X = P^+$, we find both

tetrahedral ($\mathbf{t-P^+}$) and planar forms ($\mathbf{p-P^+}$) to be minima on their PES with $\mathbf{t-P^+}$ lying lower in energy than $\mathbf{p-P^+}$ by 5.2 kcal/mol. A transition state that connects the tetrahedral and planar minima was identified. Additionally, complete active space self-consistent field (CASSCF) calculations were performed in order to examine the static correlation effect. The CASSCF energies were in satisfactory agreement with the MP2 values (Refer Tables S3 and S4 for results and associated discussion in the supporting information). The seemingly less difference between the tetrahedral and planar forms compared to most other systems that have been reported so far can be understood based on the energy decomposition analysis - natural orbital for chemical valence (EDA-NOCV) calculations^{57,58} (See Table S5 in the supporting information). We further calculated PESs for the variation of the angle between two planes formed by two 3-membered rings (referred to as ϕ in the rest of the manuscript) and are given in Figure 1b. For $X = \text{Si}$ and Al^- , PESs indicate the possibility of transition between tetrahedral forms via a planar transition state. Also for the first time we show an example of a system ($X = \text{P}^+$) where both tetrahedral and planar structures are minima, and the transition between tetrahedral forms proceeds via a planar intermediate. Accordingly, if we could design a molecular species with a chiral central atom with similar energetics, seamless transitions among four different isomers (R) and (S) for tetrahedral form, and (Z) and (E) for planar form are viable (See later).

Earlier studies on spiro- $(\text{C})_4\text{X}$ systems with planar central atoms,^{55,59} indicated that those molecules are kinetically unstable due to facile ring opening reaction corresponding to the XCC-ring ($\mathbf{r-X}$ and $\mathbf{r^*-X}$ in Figure 2a). For example, when $X = \text{C}$, the planar form was found to be a minimum and the tetrahedral form was found to be a second-order saddle point. However, the ring-opened product was found to lie lower in energy than the planar minimum by 31.7 kcal/mol with a barrier of only 2.1 kcal/mol.⁵⁵ In order to examine how competitive the ring opening process is with respect to the stereomutation process involving molecules in this study, we calculated the energetics corresponding to the ring opening pathway. The energy barriers for this process were calculated to be 11.3 and 9.0 kcal/mol for Si and Al^- systems, respectively which are higher than those calculated for the stereomutation process (4.8 and 3.7 kcal/mol, respectively). Notably, the ring-opened products are located in a very shallow region of the PES with barriers of only 0.6 and 0.1 kcal/mol, respectively for going back to the spiro structure indicating optimal kinetic stability of these species. In case of the phosphonium moiety ($X = \text{P}^+$), the barriers for transitions between tetrahedral and planar minima, and the ring opening process are comparable at 5.6 kcal/mol. For computing PESs, we considered geometrical parameters, ϕ , that measures the deviation from the planarity along the stereomutation pathway for interconversion of tetrahedral and planar forms and θ , $\angle X\text{-C1-C2}$ representing the ring opening pathway. The different tetrahedral ($\mathbf{t-X}$ and $\mathbf{t^*-X}$), planar ($\mathbf{p-X}$ and $\mathbf{p^*-X}$) and ring-opened forms ($\mathbf{r-X}$ and $\mathbf{r^*-X}$) along with the schematic representation of where these species lie on the PESs consisting the two chosen coordinates are given in Figure 2a and 2b, respectively. The PESs for $X = \text{Si}$ and Al^- (Figure 2c and 2d) clearly indicate that the stereomutation process is more

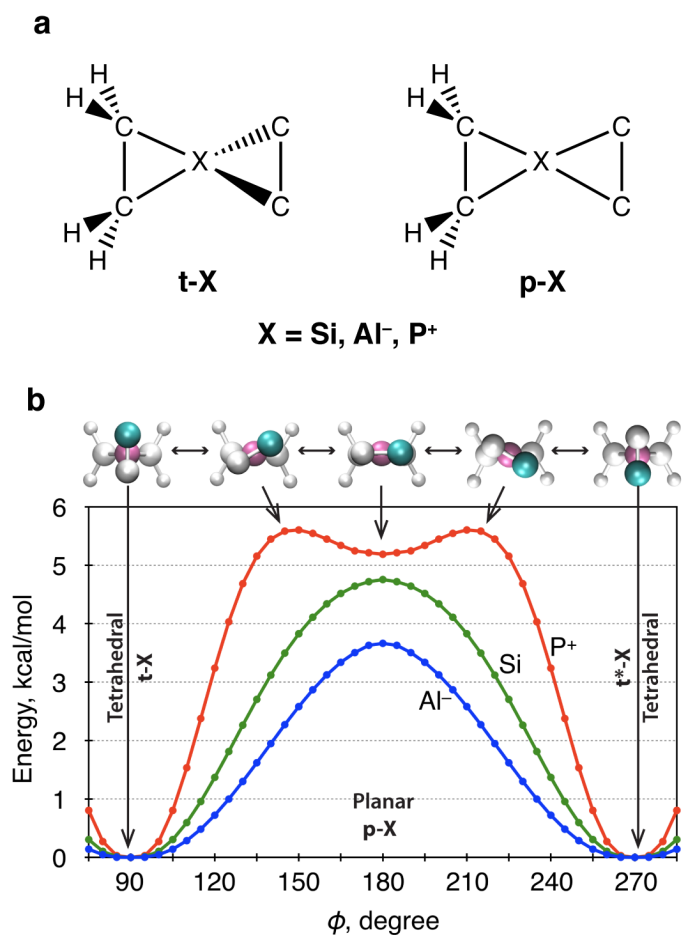


Fig. 1 a, The tetrahedral ($\mathbf{t-X}$) and planar ($\mathbf{p-X}$) forms of the XC_4H_4 moiety considered in this study. **b**, Energy (kcal/mol) change corresponding to the transition between two tetrahedral forms via a planar transition state ($X = \text{Si}$ & Al^-) or a planar intermediate structure ($X = \text{P}^+$) w.r.t. the angle (ϕ , degree) between the two planes formed by the three-membered rings as the reaction coordinate calculated at the MP2/cc-pVTZ level of theory. The structures corresponding to key values of ϕ and their positions on the PES are also given. The two carbon atoms that form the XCC ring are colored differently (silver and cyan) to distinguish the two, and the central atom X is represented in magenta color.

facile than the ring opening process and hence the system is expected to undergo the racemization reaction more favorably than ring opening. On the other hand, as noted earlier, the PES of $X = \text{P}^+$ (Figure 2e) exhibits a low energy minimum corresponding to the tetrahedral form and a high energy minimum corresponding to the planar form separated by a barrier that is comparable to the ring opening barrier. This reveals possible competition between the two pathways. We present below the dynamics of the racemization and ring opening reactions.

The foregoing discussion indicates that racemization may be possible by a simple rotation about the central tetracoordinated atom without having to necessarily break one of the covalent bonds. We investigated the atomic-level mechanisms and the dynamics of the racemization and ring opening reaction pathways using *ab initio* quasi-classical trajectory simulations⁶⁰ at the MP2/cc-pVTZ level of theory. Sets of 50 trajectories for each system were initiated from the reactant region using a microcanoni-

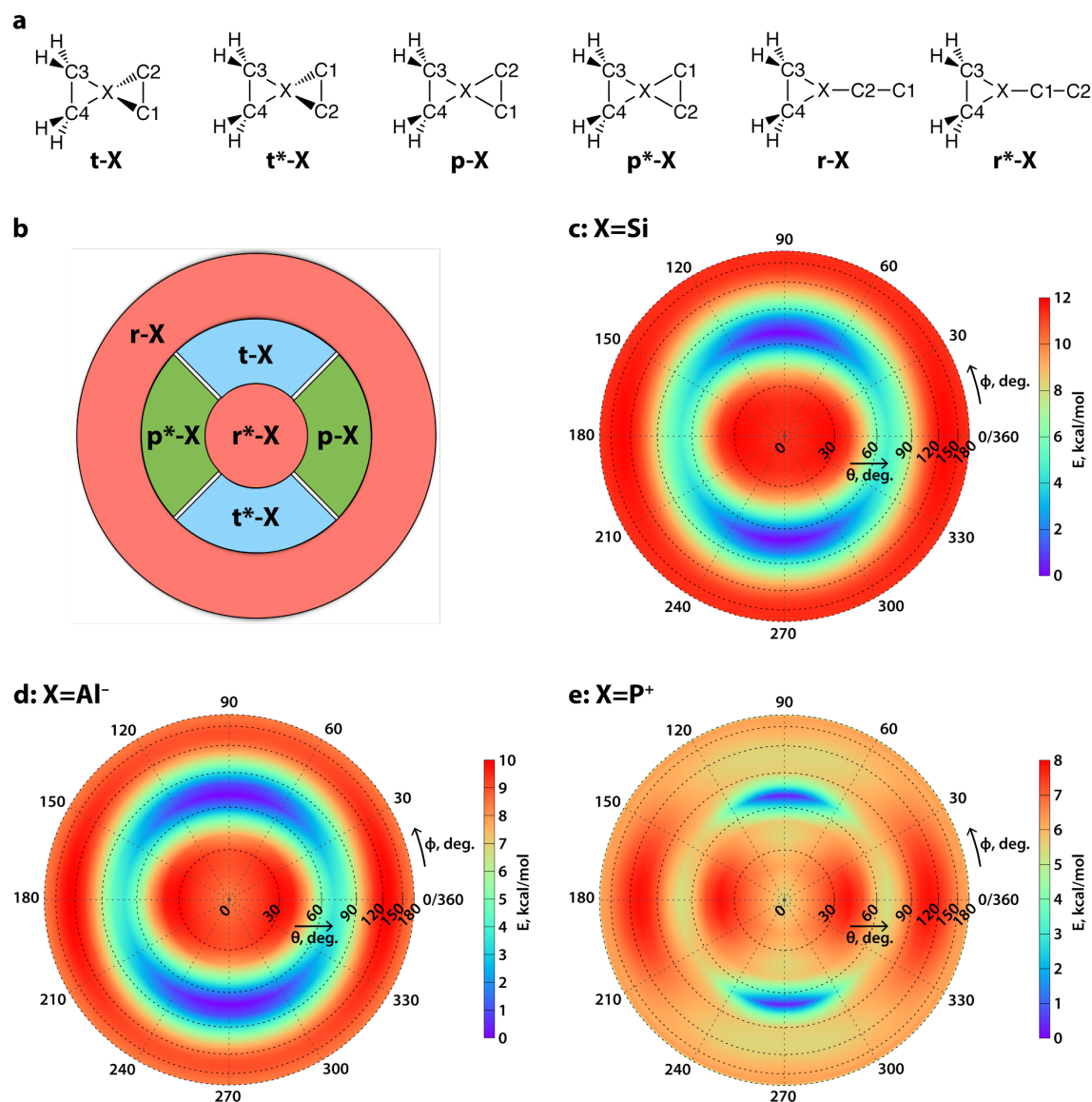


Fig. 2 PESs of the three systems indicating possible racemization process. **a**, Schematic representation of the structures of the tetrahedral (t-X and t*-X), planar (p-X and p*-X) and ring-opened (r-X and r*-X) states examined on the PESs. **b**, Schematic representation of the PES given in **c**, **d** and **e**. Approximate regions of locations of six different species shown in **a** on the PES are also indicated. **c**, **d**, and **e**, Potential energy surfaces corresponding to the transitions among the tetrahedral, planar and the ring-opened states calculated as a function of the angle between two three-membered rings (ϕ , degree), and the \angle X-C1-C2 (θ , degree) for X = Si, Al⁻ and P⁺ respectively obtained at the MP2/cc-pVTZ level of theory. The θ , radial axis is scaled using a nonlinear function for clarity.

cal ensemble with a total energy corresponding to the sum of average vibrational and rotational energies assuming a Boltzmann distribution at 300 K. The total energies available from the classical minima of the reactants were 40.8, 40.9, and 43.0 kcal/mol for Si, Al⁻, and P⁺ systems, respectively. All the trajectories were integrated for 2 ps each. Out of these 150 trajectories, 5, 28, and 35 were reactive for X = Si, Al⁻, and P⁺, respectively; i.e. they showed either racemization or ring opening reaction. The trajectories were analyzed along the θ and ϕ coordinates as defined above and a representative trajectory for each system is given in Figure 3. Racemization was observed in 4 out of 5, 27 out of 28 and 4 out of 35 reactive trajectories for X = Si, Al⁻, and P⁺ respectively (See Figure S3, S4 and S5 in the supporting informa-

tion). We can see that for X = Si and Al⁻ systems, the trajectories initially scan through the reactant region of the PES before the stereomutation process. In addition, we can observe multiple isomerizations happen including recrossing of trajectories. For X = P⁺, due to a larger barrier for stereomutation pathway, the trajectory exhibits less events of stereomutation within the integration time of 2 ps. As anticipated based on the barrier heights (Figure 2), P⁺ system exhibited more ring opening events and is negligible for the other two compared to the number of racemization events. It is interesting to note that although the barriers for the racemization and the ring opening pathways are similar, 31 trajectories followed the latter pathway and only 4 followed the former indicating the dynamical nature of the process. This

clearly indicates the role of intramolecular vibrational energy redistribution in the reaction, that can be qualitatively understood from the change of the vibrational frequencies along the reaction path (See Figure S6 in the supporting information).⁶¹ The Rice-Ramsperger-Kassel-Marcus (RRKM) lifetimes for the racemization (0.25 ps) and ring opening (0.10 ps) pathways for $X=P^+$ are consistent with the above observation. For the $X = Si$ and Al^- systems, the ring-opening lifetimes are longer compared to the racemization lifetimes owing to higher energy barriers for the ring-opening process. However, it should be noted that dynamics of the racemization is non-RRKM with several trajectories exhibiting recrossing (For details, see Table S1 in the supporting information).

In order to understand the kinetics of these transitions and average lifetimes of the different forms identified here along the stereomutation and dissociation pathways, unbiased long molecular dynamics simulations would be ideal. Performing such simulations at the MP2 level is not practical even with the best of the computational facilities and hence we have performed BOMD simulations at the DFT/BLYP level using the Goedecker⁵¹ type effective core potentials in the plane wave basis. Unfortunately, the lower BLYP level of theory underestimates the ring opening barriers and the energies of the ring-opened product compared to the MP2 and CCSD(T) methods especially for Al^- and P^+ systems, and hence only Si system is discussed here. A 400 ps long BOMD simulation on the Si system was performed and the probability distributions of geometrical parameters, ϕ and θ are presented in Figure 4a. Maximum sampling was observed for the tetrahedral forms compared to the planar or the ring-opened states consistent with the quantum mechanical calculations and quasi-classical trajectory simulations presented above. Analysis of the MD trajectory indicates that the C_4SiH_4 molecule was present in the ring-closed state for 90% of the simulation time with the number of racemization events observed during the 400 ps time to be 148. A movie representing a part of the trajectory where inter-conversions between two identical tetrahedral forms via a planar transition state is given in Section 4 of the supporting information. Such a comprehensive sampling of all possible states corresponding to the above mentioned two processes enabled us to estimate the kinetic properties of the events and the average lifetimes of each of these species.

The continuous-time Markov model on a finite state space from discrete-time data was used to model dynamical events involved in the transition among various metastable states of the $Si(C)_4H_4$ molecule. We have used the MSMBuilder3.8 software package^{62–65} to construct a Markov state model (MSM) using the BOMD simulation data at a finite time interval. BOMD conformations were clustered into fewer “microstates” identified based on the *ab initio* calculations, e.g., closed (\mathbf{t} , \mathbf{t}^* and \mathbf{p} , \mathbf{p}^*) and ring-opened (\mathbf{r} , \mathbf{r}^*) states (See Section 4.1 in the supporting information). The number of transitions between “microstates” at an interval of a certain lag time \mathcal{L} were obtained from the transition probability matrix $\mathbf{T}(\mathcal{L})$. The transition probability of a process X going from one state i to another j was calculated as

$$\mathbf{T}(\mathcal{L})_{ij} = P(X(t + \mathcal{L}) = j | X(t) = i) \quad (1)$$

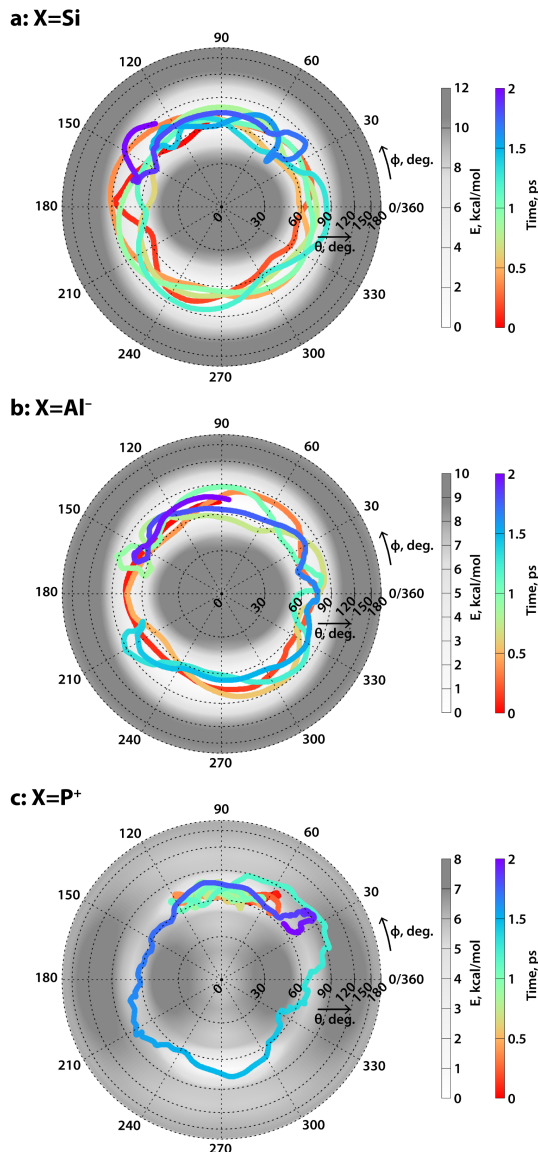


Fig. 3 Stereomutation as observed in the *ab initio* quasi-classical trajectory calculations. The time evolution of the three systems **a** ($X = Si$), **b** ($X = Al^-$) and **c** ($X = P^+$) in a representative quasi-classical trajectory calculation performed using the MP2/cc-pVTZ method initiated at the tetrahedral region. The path of the trajectory is color coded based on the time of the simulation in ps (0→2 corresponding red→blue). The time evolution is overlaid on the corresponding PES of the three systems given in monochrome. The θ , radial axis is scaled using a nonlinear function for clarity.

The time-evolution of the probability of a process in a given state is obtained as,

$$\frac{dP(t)}{dt} = \mathbf{K} P(t) \quad (2)$$

$P(t)$ is the probability of a process at time t ; \mathbf{K} is the rate matrix, and $\mathbf{T}(\mathcal{L})$ is given by the matrix exponential as⁶², $\mathbf{T}(\mathcal{L}) = \exp(\mathbf{K}\mathcal{L})$.

The Markov time, the time scale at which the model is Markovian, a crucial step for an MSM, is achieved by examining the implied time scales at different lag times. At a given \mathcal{L} , the im-

plied time scale t_k can be calculated as⁶⁶,

$$t_k(\mathcal{L}) = -\frac{\mathcal{L}}{\ln |\lambda_k(\mathcal{L})|} \quad (3)$$

where, λ_k is k^{th} eigenvalue of the estimated transition matrix at \mathcal{L} . If the model is Markovian at lag time \mathcal{L} , implied time scales should remain constant while using longer lag times, e.g., at $k\mathcal{L}$, when $k\mathcal{L} > \mathcal{L}$ (See Figure S8 in the supporting information). In order to validate the results obtained from implied timescales, we performed Chapman-Kolmogorov (CK) test which follows, $\mathbf{T}(\mathcal{L})^k \approx \mathbf{T}(k\mathcal{L})$, using the PyEMMA package⁶⁶ where, $\mathbf{T}(\mathcal{L})$ and $\mathbf{T}(k\mathcal{L})$ indicate transition matrices estimated at lag time of \mathcal{L} and $k\mathcal{L}$, respectively. The transition rates along the two pathways are given in Figure 4b. We found the rate of ring closing (0.72 ps^{-1}) to be an order of magnitude faster than that of ring opening (0.06 ps^{-1}) indicating that the equilibrium is shifted towards the spiro-X structure even when calculated using a slightly underestimated barrier for ring opening using the BLYP functional.

The mean lifetimes were computed from the dwell time distributions of various states.⁶⁷ $P_{dwell}(t; t_d^*)$ is the probability that a dwell has a duration of time t considering a transient disruption time (relaxation) t_d^* and can be defined as

$$P_{dwell}(t; t_d^*) = \frac{1}{N_{dwell}} \sum_{i=1}^{N_{dwell}} \partial[\tau_i(t_d^*) - t] \quad (4)$$

So, depending on the value of t_d^* , we can ignore the transient disruption and reassociation processes. If a dwell, is disrupted and then again reassociated with a time-difference, of say, Δt , and, if $\Delta t > t_d^*$ the dwell is considered as a new event, else it is still a part of the same dwell. $\partial[\tau_i(t_d^*) - t]$ is a delta function:

$$\partial[\tau_i(t_d^*) - t] = \begin{cases} 0, & \text{if } \tau_i(t_d^*) \neq t \\ 1, & \text{if } \tau_i(t_d^*) = t \end{cases}$$

$\tau_i(t_d^*)$ is the time duration for the i^{th} dwell. So, $\tau_i(t_d^*) = t$, if $t \leq \tau_i(t_d^*) \leq t + dt$. dt is the width of the histogram distribution class intervals. $S(t; t_d^*)$ denotes the survival probability that a dwell will survive even after time-length of t for a given t_d^* transient disruption time

$$S(t; t_d^*) = 1 - \int_0^t d\tau P(\tau, t_d^*) \quad (5)$$

The mean dwell time, i.e., the mean lifetime of each state at a given t_d^* can be expressed as

$$\langle \tau(t_d^*) \rangle = \int_0^\infty dt S(t; t_d^*) \quad (6)$$

The most interesting aspect is that the racemization process was found to be occurring at the rate of about 0.4 ps^{-1} . Figure 4c shows that the average lifetimes of the spiro-X, calculated directly from the BOMD trajectory following the protocol which was applied in case of MD trajectories⁶⁷, is also calculated to be significantly longer ($\sim 7 \text{ ps}$) than the ring-opened states ($\sim 1 \text{ ps}$). More details of the lifetime calculations are given in the supporting in-

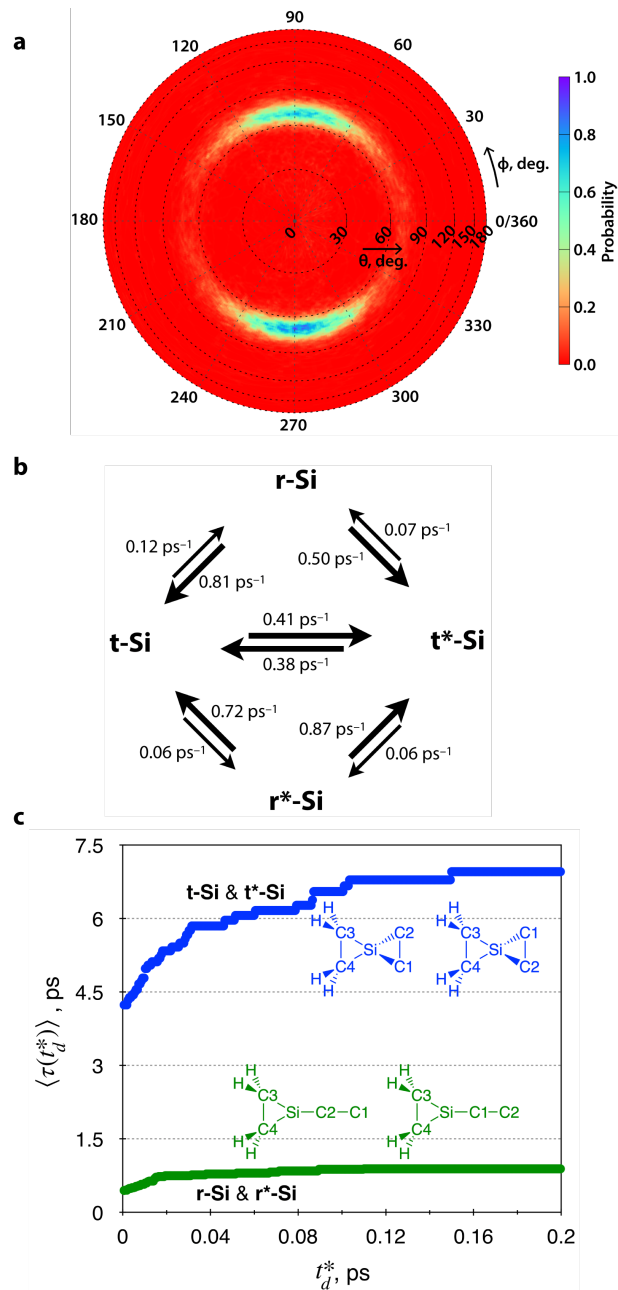


Fig. 4 Extensive sampling of the racemization process, kinetics and lifetime calculations on the $\text{Si}(\text{C})_4\text{H}_4$ molecule calculated using the BOMD simulations. **a**, Probability distribution corresponding to the change in the angle between two three-membered rings (ϕ , degree), and the $\angle \text{X}-\text{C}1-\text{C}2$ (θ , degree) showing the maximum sampling in the tetrahedral states and possible racemization transition via the planar structure. Log scale is used for the radial axis for clarity. **b**, Transition rates between tetrahedral structures (**t-Si** and **t*-Si**) via planar transition states (**p-Si** and **p*-Si**), and rates for the transitions between the tetrahedral structures (**t-Si** and **t*-Si**) and ring-opened states (**r-Si** and **r*-Si**) obtained using MSM analysis. **c**, Mean lifetimes of tetrahedral (blue) and ring-opened (green) states calculated using different transient disruption times t_d^* .

formation (See Section 4.2).

We then set out to identify a true chiral system that has unique (R) and (S) configurations for which both the tetrahedral and pla-

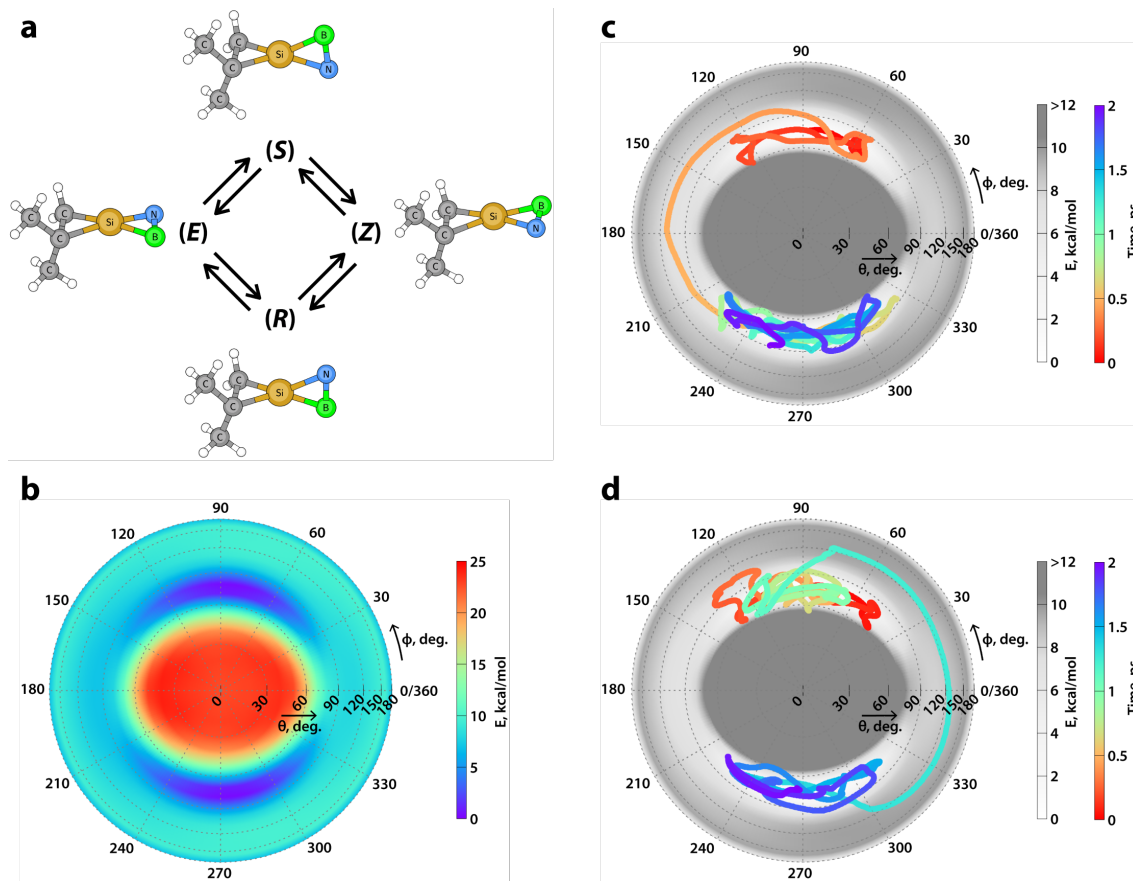


Fig. 5 Racemization of a true chiral system via a planar intermediate structure. **a**, Schematic representation of the structures of the tetrahedral (*R*) and (*S*) isomers and possible transition between them via one of the planar intermediate structures (*Z*) or (*E*). **b**, PES of the chiral system with respect to the two angles (θ and ϕ) calculated at the MP2/cc-pVTZ level showing two deep minima for (*R*) and (*S*) stereoisomers and two shallow minima for (*Z*) and (*E*) isomers. **c**, and **d**, The time evolution of the chiral structure initiated at (*S*) region obtained using the *ab initio* quasi-classical trajectory simulations done at the MP2/6-31+G(d) level of theory. In **c**, (*S*) to (*R*) isomerization proceeds via the (*E*) isomer, whereas in **d**, the transition proceeds via the (*Z*) isomer. The time evolution from 0→2 ps is represented by color coding from red→blue. The θ , radial axis is scaled using a nonlinear function for clarity.

nar forms are minima on its PES. Well over 100 different molecular species with chiral Si, P⁺ and Al⁻ centers were conceived and calculations were performed on their planar and tetrahedral forms. Similar to the parent molecules (Figure 1a), geometry optimization and frequency calculations were done at the MP2/cc-pVTZ level of theory. We present here a neutral chiral molecule with a Si center, [Si(C₂NB)H₂(CH₃)₂], whose tetrahedral and planar forms are minima (See Figure S11 in the supporting information). Since the molecule is asymmetric about the central Si atom, the two stereoisomers are isoenergetic. However, the two planar forms are different and hence have different stabilities (analogous to *cis* and *trans* forms of an alkene). We can conveniently use the (*Z*) and (*E*) nomenclature for the planar forms (structures of the four isomers are given in Figure 5a). The PES of these molecules with respect to θ and ϕ are given in the Figure 5b and their locations on the PES are indicated in Figure 5a. Starting from the *S* isomer, clockwise rotation of the three-membered Si-B-N ring with respect to the other ring would lead to the (*R*) stereoisomer via the (*Z*) isomer. On the other hand, anti-clockwise rotation from the (*S*) isomer would give the (*R*) isomer via the (*E*) isomer. The (*Z*) and (*E*) planar forms are 8.0 kcal/mol and 7.0 kcal/mol

higher in energy compared to the tetrahedral ((*R*) and (*S*)) (See Figure S11 in the supporting information) forms. The two planar forms were found to be in shallow minima that would enable them to convert to the tetrahedral states instantaneously. The Si-B bond length of the planar forms (*Z*) and (*E*) are found to be elongated by about 0.5 and 0.3 Å respectively, compared to the tetrahedral forms. Hence the positions of the minima of the planar states and the corresponding transitions in the trajectories are shifted towards slightly larger θ values (See below). The ring-opened intermediate along the Si-N bond lies 22.6 kcal/mol higher in energy relative to the tetrahedral form. Whereas, the other ring-opened structure along the Si-B bond is not a minimum on its PES. In the Figure S11 of the supporting information, we have reported one such structure lying 9.9 kcal/mol higher in energy w.r.t. the tetrahedral form on the PES. We also performed the *ab initio* quasi-classical trajectory simulations on this system at the MP2/6-31+G(d) level. Among 45 calculations initiated at the reactant region (*S* isomer), 5 were reactive, out of which, 4 exhibited racemization reactions without bond breaking (See Figure S12 and S13 in the supporting information). Two representative trajectories are given in Figure 5c and 5d, which show that

the molecule goes from the (*S*) to (*R*) isomer via the (*E*) and (*Z*) isomers, respectively. In summary, the energetic and dynamical considerations of this novel chiral system clearly point to stereoinversion upon rotation about the asymmetric atom and hence provides a fundamental model that exhibit such phenomenon. Experimental determination of molecules containing planar tetracoordinate Si⁶⁸ and P^{+26,69} have been reported before and hence we hope that it is possible to realize these and/or related molecular systems.

4 Conclusions

We have identified new spiro-(C)₄X (X = Si, Al⁻ and P⁺) analogues that exhibit two hitherto unknown phenomena: (a) racemization reaction via a planar transition state and (b) racemization reaction via a planar intermediate state, both via rotation about the central atom. State of the art theoretical calculations (electronic structure calculations, *ab initio* quasi-classical trajectory calculations and BOMD simulations) were done to rigorously characterize the thermodynamic, kinetic and dynamic properties. A true chiral neutral molecule is shown to undergo transitions between (*S*) and (*R*) isomers via proposed (*E*) or (*Z*) forms. Based on long unbiased BOMD simulations, we estimate this racemization process to happen at sub-picosecond timescale. We are confident that this study will inspire further activity in this area in terms of expanding the chemical search space to unravel novel molecules where transitions between stable planar and tetrahedral forms are feasible. Firstly, this will enhance our understanding of the boundaries of established chemical concepts beyond which they breakdown. Secondly, experimental realization of such novel chemical entities may result in innovative applications in broader fields of science and technology.

Conflicts of interest

There are no conflicts of interest to declare.

Acknowledgements

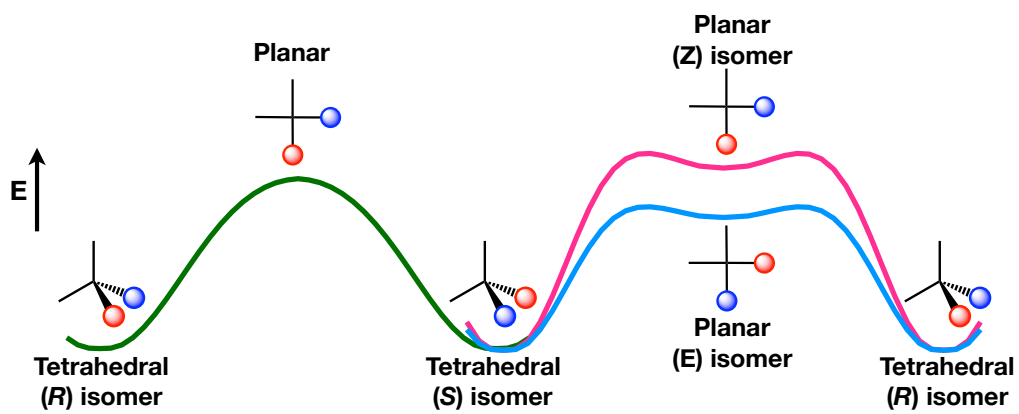
We thank Prof. Roald Hoffmann, Prof. Gernot Frenking and Prof. G. Narahari Sastry for fruitful discussions, and Dr. Semparithi Aravindan for his help in making the movie included in the supporting information. UDP thanks DST-SERB (Grant No. EMR/2016/007697) for financial assistance. SR thanks DST-SERB (Grant No. PDF/2018/000142) for the National Postdoctoral Fellowship.

Notes and references

- 1 J. van't Hoff, *Arch. Neerl. Sci. Exactes Nat*, 1874, 445–454.
- 2 J. A. Le Bel, *Bull. Soc. Chim. Fr*, 1874, **22**, 337–347.
- 3 H. Wynberg, G. Hekkert, J. Houbiers and H. Bosch, *J. Am. Chem. Soc.*, 1965, **87**, 2635–2639.
- 4 H. Monkhorst, *Chem. Commun.*, 1968, 1111–1112.
- 5 R. Hoffmann, R. W. Alder and C. F. Wilcox Jr, *J. Am. Chem. Soc.*, 1970, **92**, 4992–4993.
- 6 J. B. Collins, J. D. Dill, E. D. Jemmis, Y. Apeloig, P. v. R. Schleyer, R. Seeger and J. A. Pople, *J. Am. Chem. Soc.*, 1976, **98**, 5419–5427.
- 7 F. A. Cotton and M. Millar, *J. Am. Chem. Soc.*, 1977, **99**, 7886–7891.
- 8 D. Röttger and G. Erker, *Angew. Chem. Int. Ed.*, 1997, **36**, 812–827.
- 9 W. Siebert and A. Gunale, *Chem. Soc. Rev.*, 1999, **28**, 367–371.
- 10 R. Keese, *Chem. Rev.*, 2006, **106**, 4787–4808.
- 11 L.-M. Yang, E. Ganz, Z. Chen, Z.-X. Wang and P. v. R. Schleyer, *Angew. Chem. Int. Ed.*, 2015, **54**, 9468–9501.
- 12 P. D. Pancharatna, M. A. Méndez-Rojas, G. Merino, A. Vela and R. Hoffmann, *J. Am. Chem. Soc.*, 2004, **126**, 15309–15315.
- 13 G. Merino, M. A. Mendez-Rojas, A. Vela and T. Heine, *J. Comput. Chem.*, 2007, **28**, 362–372.
- 14 M. J. Pepper, I. Shavitt, P. V. R. Schleyer, M. N. Glukhovtsev, R. Janoschek and M. Quack, *J. Comput. Chem.*, 1995, **16**, 207–225.
- 15 M. P. McGrath and L. Radom, *J. Am. Chem. Soc.*, 1993, **115**, 3320–3321.
- 16 D. R. Rasmussen and L. Radom, *Angew. Chem. Int. Ed.*, 1999, **38**, 2875–2878.
- 17 C. Zhang, W. Sun and Z. Cao, *J. Am. Chem. Soc.*, 2008, **130**, 5638–5639.
- 18 Y. Pei and X. C. Zeng, *J. Am. Chem. Soc.*, 2008, **130**, 2580–2592.
- 19 C. H. Suresh and G. Frenking, *Organometallics*, 2010, **29**, 4766–4769.
- 20 K. Thirumoorthy, A. Karton and V. S. Thimmakonda, *J. Phys. Chem. A*, 2018, **122**, 9054–9064.
- 21 O. Yañez, A. Vásquez-Espinal, R. Pino-Rios, F. Ferraro, S. Pan, E. Osorio, G. Merino and W. Tiznado, *Chem. Commun.*, 2017, **53**, 12112–12115.
- 22 M. W. Wong and L. Radom, *J. Am. Chem. Soc.*, 1989, **111**, 1155–1156.
- 23 Z.-X. Wang and P. v. R. Schleyer, *J. Am. Chem. Soc.*, 2002, **124**, 11979–11982.
- 24 J. Xu, X. Zhang, S. Yu, Y.-h. Ding and K. H. Bowen, *J. Phys. Chem. Lett.*, 2017, **8**, 2263–2267.
- 25 M. Driess, J. Aust, K. Merz and C. van Wüllen, *Angew. Chem. Int. Ed.*, 1999, **38**, 3677–3680.
- 26 V. Chandrasekhar, *Resonance*, 2001, **6**, 84–90.
- 27 S.-D. Li, G.-M. Ren, C.-Q. Miao and Z.-H. Jin, *Angew. Chem. Int. Ed.*, 2004, **43**, 1371–1373.
- 28 H.-b. Xie and Y.-h. Ding, *J. Chem. Phys.*, 2007, **126**, 184302.
- 29 L.-S. Wang, A. I. Boldyrev, X. Li and J. Simons, *J. Am. Chem. Soc.*, 2000, **122**, 7681–7687.
- 30 A. I. Boldyrev and L.-S. Wang, *J. Phys. Chem. A*, 2001, **105**, 10759–10775.
- 31 E. D. Jemmis and P. Parameswaran, *Chem. Eur. J.*, 2007, **13**, 2622–2631.
- 32 Y. Li, F. Li, Z. Zhou and Z. Chen, *J. Am. Chem. Soc.*, 2011, **133**, 900–908.
- 33 H.-F. Zheng, J. Xu and Y.-H. Ding, *J. Comput. Chem.*, 2020, **41**, 119–128.

- 34 N. Job, A. Karton, K. Thirumoorthy, A. L. Cooksy and V. S. Thimmakonda, *J. Phys. Chem. A*, 2020, **124**, 987–1002.
- 35 K. Exner and P. von Ragué Schleyer, *Science*, 2000, **290**, 1937–1940.
- 36 Z.-X. Wang and P. von Ragué Schleyer, *Science*, 2001, **292**, 2465–2469.
- 37 Z.-X. Wang and P. v. R. Schleyer, *Angew. Chem. Int. Ed.*, 2002, **41**, 4082–4085.
- 38 R. Islas, T. Heine, K. Ito, P. v. R. Schleyer and G. Merino, *J. Am. Chem. Soc.*, 2007, **129**, 14767–14774.
- 39 B. B. Averkiev, D. Y. Zubarev, L.-M. Wang, W. Huang, L.-S. Wang and A. I. Boldyrev, *J. Am. Chem. Soc.*, 2008, **130**, 9248–9250.
- 40 T. Heine and G. Merino, *Angew. Chem. Int. Ed.*, 2012, **51**, 4275–4276.
- 41 V. Vassilev-Galindo, S. Pan, K. J. Donald and G. Merino, *Nat. Rev. Chem.*, 2018, **2**, 0114.
- 42 H. Zhang, Y. Li, J. Hou, K. Tu and Z. Chen, *J. Am. Chem. Soc.*, 2016, **138**, 5644–5651.
- 43 R. A. Kendall, T. H. Dunning Jr and R. J. Harrison, *J. Chem. Phys.*, 1992, **96**, 6796–6806.
- 44 M. J. Frisch, G. W. Trucks, H. B. Schlegel, G. E. Scuseria, M. A. Robb, J. R. Cheeseman, G. Scalmani, V. Barone, B. Mennucci, G. A. Petersson, H. Nakatsuji, M. Caricato, X. Li, H. P. Hratchian, A. F. Izmaylov, J. Bloino, G. Zheng, J. L. Sonnenberg, M. Hada, M. Ehara, K. Toyota, R. Fukuda, J. Hasegawa, M. Ishida, T. Nakajima, Y. Honda, O. Kitao, H. Nakai, T. Vreven, J. A. Montgomery, Jr., J. E. Peralta, F. Ogliaro, M. Bearpark, J. J. Heyd, E. Brothers, K. N. Kudin, V. N. Staroverov, R. Kobayashi, J. Normand, K. Raghavachari, A. Rendell, J. C. Burant, S. S. Iyengar, J. Tomasi, M. Cossi, N. Rega, J. M. Millam, M. Klene, J. E. Knox, J. B. Cross, V. Bakken, C. Adamo, J. Jaramillo, R. Gomperts, R. E. Stratmann, O. Yazyev, A. J. Austin, R. Cammi, C. Pomelli, J. W. Ochterski, R. L. Martin, K. Morokuma, V. G. Zakrzewski, G. A. Voth, P. Salvador, J. J. Dannenberg, S. Dapprich, A. D. Daniels, ö. Farkas, J. B. Foresman, J. V. Ortiz, J. Cioslowski and D. J. Fox, *Gaussian 09 Revision C.01*, 2009, Gaussian Inc. Wallingford CT.
- 45 U. Lourderaj, K. Song, T. L. Windus, Y. Zhuang and W. L. Hase, *J. Chem. Phys.*, 2007, **126**, 044105.
- 46 U. Lourderaj, R. Sun, S. C. Kohale, G. L. Barnes, W. A. de Jong, T. L. Windus and W. L. Hase, *Comput. Phys. Commun.*, 2014, **185**, 1074–1080.
- 47 M. Valiev, E. Bylaska, N. Govind, K. Kowalski, T. Straatsma, H. V. Dam, D. Wang, J. Nieplocha, E. Apra, T. Windus and W. de Jong, *Comput. Phys. Commun.*, 2010, **181**, 1477–1489.
- 48 W. L. Hase and D. G. Buckowski, *Chem. Phys. Lett.*, 1980, **74**, 284–287.
- 49 W. C. Swope, H. C. Andersen, P. H. Berens and K. R. Wilson, *J. Chem. Phys.*, 1982, **76**, 637–649.
- 50 J. Hutter, *Car-Parinello Molecular Dynamics: An ab initio electronic structure and molecular dynamics program*, <http://www.cpmo.org/>.
- 51 S. Goedecker, M. Teter and J. Hutter, *Phys. Rev. B*, 1996, **54**, 1703–1710.
- 52 L. Kleinman and D. M. Bylander, *Phys. Rev. Lett.*, 1982, **48**, 1425–1428.
- 53 C. Lee, W. Yang and R. G. Parr, *Phys. Rev. B*, 1988, **37**, 785–789.
- 54 A. D. Becke, *Phys. Rev. A*, 1988, **38**, 3098–3100.
- 55 U. D. Priyakumar, A. S. Reddy and G. N. Sastry, *Tetrahedron Lett.*, 2004, **45**, 2495–2498.
- 56 R. Hoffmann, *Pure Appl. Chem.*, 1971, **28**, 181–194.
- 57 M. v. Hopffgarten and G. Frenking, *Wiley Interdisciplinary Reviews: Computational Molecular Science*, 2012, **2**, 43–62.
- 58 G. Frenking and F. M. Bickelhaupt, *The Chemical Bond*, 2014, **1**, 121–158.
- 59 B. Sateesh, A. Srinivas Reddy and G. Narahari Sastry, *J. Comput. Chem.*, 2007, **28**, 335–343.
- 60 S. Pratihar, X. Ma, Z. Homayoon, G. L. Barnes and W. L. Hase, *J. Am. Chem. Soc.*, 2017, **139**, 3570–3590.
- 61 M. Gruebele and P. Wolynes, *Acc. Chem. Res.*, 2004, **37**, 261–267.
- 62 R. T. McGibbon and V. S. Pande, *J. Chem. Phys.*, 2015, **143**, 034109.
- 63 M. P. Harrigan, M. M. Sultan, C. X. Hernández, B. E. Husic, P. Eastman, C. R. Schwantes, K. A. Beauchamp, R. T. McGibbon and V. S. Pande, *Biophys. J.*, 2017, **112**, 10–15.
- 64 B. E. Husic and V. S. Pande, *J. Am. Chem. Soc.*, 2018, **140**, 2386–2396.
- 65 J. Kalbfleisch and J. F. Lawless, *J. Am. Stat. Assoc.*, 1985, **80**, 863–871.
- 66 M. K. Scherer, B. Trendelkamp-Schroer, F. Paul, G. Pérez-Hernández, M. Hoffmann, N. Plattner, C. Wehmeyer, J.-H. Prinz and F. Noé, *J. Chem. Theory Comput.*, 2015, **11**, 5525–5542.
- 67 S. Goyal, A. Chattopadhyay, K. Kasavajhala and U. D. Priyakumar, *J. Am. Chem. Soc.*, 2017, **139**, 14931–14946.
- 68 F. Ebner and L. Greb, *J. Am. Chem. Soc.*, 2018, **140**, 17409–17412.
- 69 M. Driess, H. Ackermann, J. Aust, K. Merz and C. von Wüllen, *Angew. Chem. Int. Ed.*, 2002, **41**, 450–453.

TOC Graphic



First examples of racemization of tetrahedral tetracoordinate centers via a planar transition state or an intermediate structure.

pccp_final.pdf (5.67 MiB)

[view on ChemRxiv](#) • [download file](#)

Supplementary Information: Transition between [R]- and [S]-Stereoisomers without Bond Breaking

Shampa Raghunathan,[†] Komal Yadav,[‡] V. C. Rojisha,[†] Tanashree Jaganade,[†] V.
Prathyusha,[†] Swetha Bikkina,[†] U. Lourderaj,^{*,‡} and U. Deva Priyakumar^{*,†}

[†]*Center for Computational Natural Sciences and Bioinformatics International Institute of
Information Technology, Hyderabad 500 032, India*

[‡]*School of Chemical Sciences, National Institute of Science Education and Research,
Bhubaneswar, India*

E-mail: u.lourderaj@niser.ac.in; deva@iiit.ac.in

1. Methods

EDA-NOCV analysis The nature of interactions between the C_2H_4X fragment and in p-X and t-X ($X = Si, Al^-$ and P^+) were analyzed by energy decomposition analysis combined with natural orbitals for chemical valence (EDA-NOCV) analysis.^[1] EDA-NOCV analysis is performed at the BP86 level of theory with a triple- ζ basis set having two sets of polarization functions with a frozen-core approximation for the core electrons (BP86/TZ2P)^[2] using ADF 2016.107 program.^[3-5]

Ab initio classical trajectory simulations Additional set of 30 trajectories for each system were calculated, which initiated in the reactant region with higher total energies of 52.28, 48.65, and 46.60 kcal/mol for Si, Al^- , and P^+ systems, respectively. The number of reactive trajectories following the racemization and the ring opening paths are given in Table S1.

Table S1: Details of trajectories showing stereomutation initiated with higher total energies.

Systems	Energy (kcal/mol)	No. of trajectories showing stereomutation	No. of trajectories showing ring opening path
$[Si(C_4)H_4]$	48.65	10	1
$[Al(C_4)H_4]^-$	52.28	20	0
$[P(C_4)H_4]^+$	46.60	2	15

2. Results of electronic structure calculations

2.1 Energies

Table S2: Relative energies of transition states/intermediates (in kcal mol⁻¹) obtained at the MP2 and CCSD(T) levels of theory using the cc-pVTZ basis set. Transition state, c[‡]-P corresponds to the closed-planar to closed-tetrahedral transition and r[‡]-X corresponds to the ring opening transition state.

Species	MP2	CCSD(T) ^a
[Si(C₄)H₄]		
p-Si	4.76	4.51
t-Si	0.00	0.00
r [‡] -Si	11.34	8.53
r-Si	11.26	8.56
[Al(C₄)H₄]⁻		
p-Al	3.66	3.52
t-Al	0.00	0.00
r [‡] -Al	8.99	7.83
r-Al	8.37	7.44
[P(C₄)H₄]⁺		
p-P	5.19	4.49
c [‡] -P	5.63	4.30
t-P	0.00	0.00
r [‡] -P	5.62	3.80
r-P	5.44	1.20

^a Values given from single point energy calculations at CCSD(T) level using the MP2 optimized geometries.

It can be seen from Tables S3 and S4 that, for **p-Si**, the MP2/cc-pVTZ level of theory gives lower energy than the CASSCF(8,8) and CASSCF(14,14) methods. Including static correlation using (8,8) active space increases the **r[‡]-Si** energy. While for **r[‡]-Si**, the MP2 energy is higher than that obtained using CASSCF methods. It should be pointed that for both **p-Si** and **r[‡]-Si** the largest deviation of MP2 energies from the CASSCF and CASPT2 values is only about 3 kcal/mol. In the case of X = P system, a similar trend was observed with MP2 energies lower than the CASSCF energies and with even smaller deviations in energies. Thus, for the ab initio dynamical simulations, the MP2/cc-pVTZ level of theory was considered.

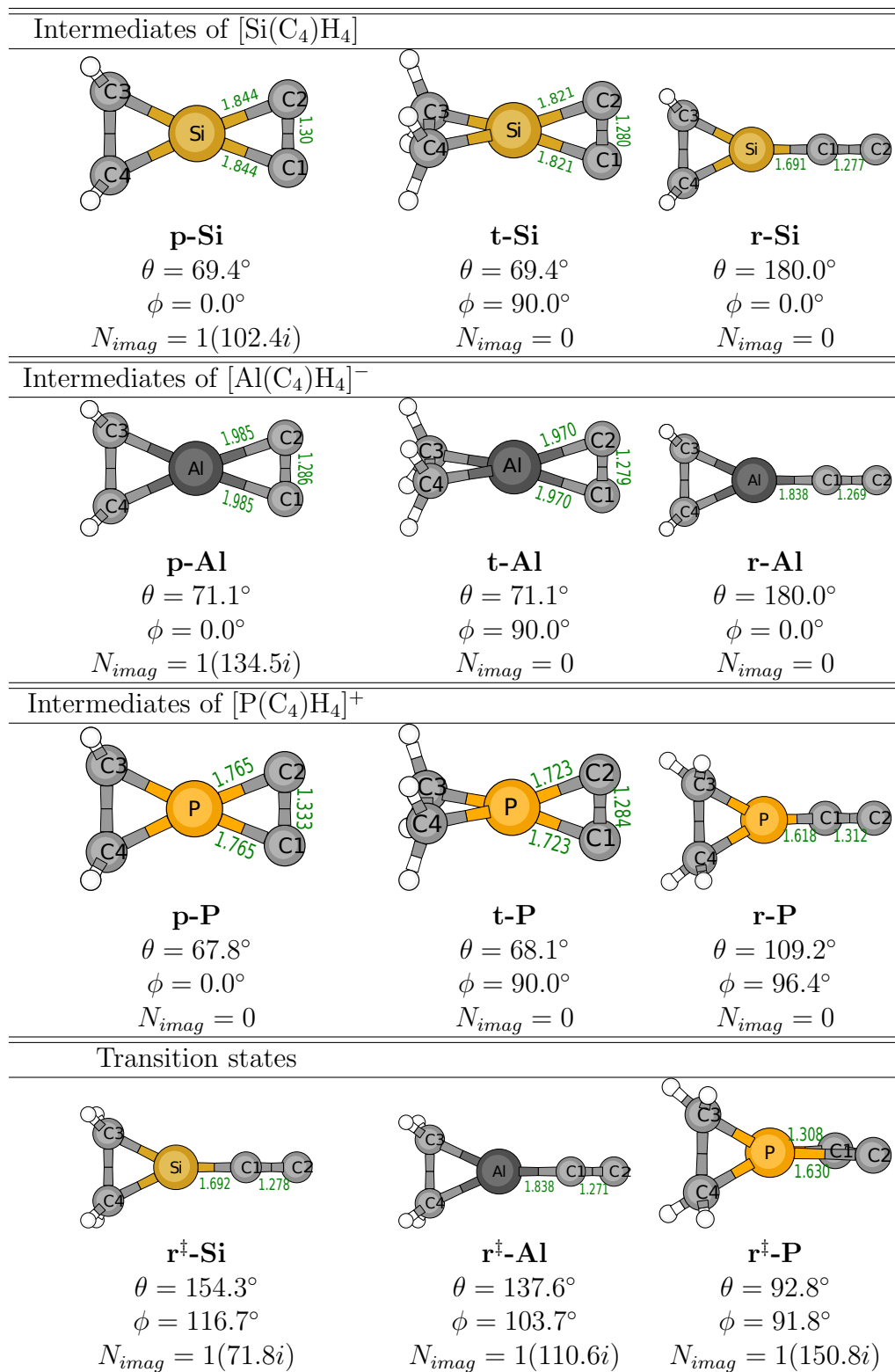
Table S3: Relative single point energies (in kcal mol⁻¹) on MP2/cc-pVTZ optimized geometries at CASSCF(8,8)/cc-pVTZ and CASPT2(8,8)/cc-pVTZ level of theories. Transition state, r[‡]-X corresponds to the ring opening transition state.

Species	MP2	CASSCF	CASPT2
[Si(C₄)H₄]			
p-Si	4.8	5.6	6.8
t-Si	0.0	0.0	0.0
r [‡] -Si	11.3	8.0	10.7

Table S4: Relative single point energies (in kcal mol⁻¹) on MP2/cc-pVTZ optimized geometries at CASSCF(14,14)/cc-pVTZ level of theory. Transition state, c[‡]-P corresponds to the closed-planar to closed-tetrahedral transition and r[‡]-X corresponds to the ring opening transition state.

Species	MP2	CASSCF
[Si(C₄)H₄]		
p-Si	4.8	6.1
t-Si	0.0	0.0
r [‡] -Si	11.3	7.9
[P(C₄)H₄]⁺		
p-P	5.2	7.0
c [‡] -P	5.6	6.1
t-P	0.0	0.0
r [‡] -P	5.6	5.3

2.2 Structures



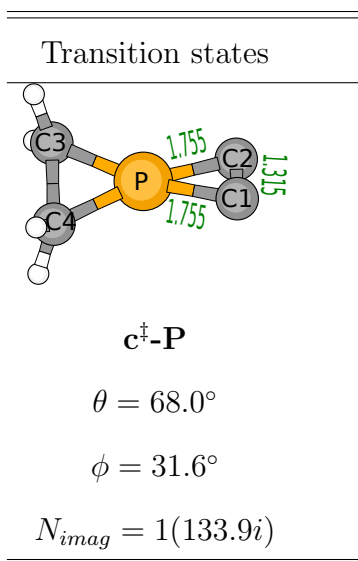


Figure S1: Optimized structures and selected geometrical parameters of planar (p-X), tetrahedral (t-X), ring-opened (r-X) minima, and transition state ($\mathbf{r^{\ddagger}\text{-X}}$) of $\text{X}(\text{C})_4\text{H}_4$ systems at MP2/cc-pVTZ level of theory; in case of $\text{X}=\text{P}^+$, the transition state ($\mathbf{c^{\ddagger}\text{-P}}$) responsible for planar to tetrahedral transition. Bond distances (in Å), angle between two three-membered rings (ϕ , degree), $\angle\text{X-C1-C2}$ (θ , degree), and N_{imag} representing number of imaginary frequency with values given in parentheses.

Bonding analysis using EDA-NOCV method In order to get a quantitative interpretation of chemical bonds to assess the stability of the planar versus tetrahedral $\text{X}(\text{C})_4\text{H}_4$ systems we have performed the EDA-NOCV analysis. To this end, the instantaneous interaction energy ΔE_{int} was computed between two fragments $\text{C}\equiv\text{C}$ and XC_2H_4 units (See Figure S2(a) for the scheme). The total interaction energy ΔE_{int} is decomposed as,

$$\Delta E_{int} = \Delta E_{Pauli} + \Delta E_{elstat} + \Delta E_{orb} \quad . \quad (1)$$

Where 1st, 2nd and 3rd terms refer to Pauli repulsion, electrostatic and orbital interaction energies, respectively; further the bond dissociation energy (by definition with opposite sign) $-D_e = (\Delta E_{int} + \Delta E_{prep})$.^[1] Here ΔE_{prep} refers to preparation energy. The best bonding situation for p-X and t-X systems inferred from these analyses are depicted in Figure S2(b), and results are given in Table S5. The EDA-NOCV results indicate that the nature of interaction of the $\text{C}\equiv\text{C}$ fragment with the remaining one varies from planar to tetrahedral compounds.

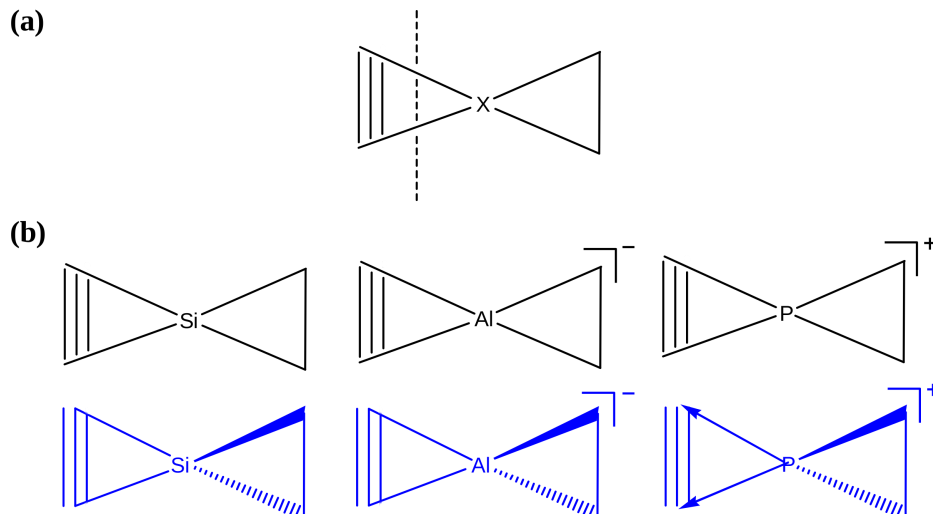


Figure S2: (a) Fragmentation scheme used for EDA-NOCV analyses. (b) Best bonding representation for p-X and t-X from EDA-NOCV analyses.

Table S5: Energy decomposition analyses (values in kcal/mol) of p-X and t-X systems at BP86/TZ2P. X=C was considered as well for comparison.

	ΔE_{int}	${}^a\Delta E_{Pauli}$	${}^a\Delta E_{elstat}$	ΔE_{orb}	ΔE_{prep}	D_e
p-C	-173.7	434.9	-213.2	-395.4	41.4	-132.3
			(35.0%)	(65.0%)		
t-C	-314.0	642.2	-332.8	-623.4	221.5	-92.5
			(34.8%)	(65.2%)		
p-Si	-174.8	264.5	-129.9	-309.4	64.7	-110.1
			(29.6%)	(70.4%)		
t-Si	-247.3	267.6	-132.7	-382.2	135.1	-112.3
			(25.8%)	(74.2%)		
p-Al	-206.6	208.2	-116.4	-298.4	56.8	-149.8
			(28.1%)	(71.9%)		
t-Al	-232.4	214.6	-117.7	-329.3	80.4	-152.0
			(26.3%)	(73.7%)		
p-P	-134.5	326.5	-118.7	-342.4	53.4	-81.1
			(25.7%)	(74.3%)		
t-P	-139.9	329.5	-93.7	-375.8	58.0	-81.9
			(20.0%)	(80.0%)		

^aValues in parenthesis give the percentage contribution to the total attractive interactions, $(\Delta E_{elstat} + \Delta E_{orb})$.

In all three cases $\Delta E_{orb} > \Delta E_{elstat}$, hence the nature of $C\equiv C \cdots XC_2H_4$ can be identified as covalent contribution to the chemical bond. Calculated EDA terms reveal that the chemical bonding in Si and Al^- systems is of electron sharing type whereas donor acceptor type in

P^+ system between two fragments. The bond dissociation energy would give an estimate of the relative strength of the $C\equiv C\cdots XC_2H_4$ interaction. Here, we see D_e in tetrahedral structures are larger than those in planar ones in all three isoelectronic systems (Si, Al^- & P^+).

3. Dynamics using classical trajectory calculations

3.1 Analysis of ab initio classical trajectories

The pathways of the stereomutation processes were analyzed by following the internal coordinates θ and ϕ along the ab initio classical trajectories.

[Si(C₄)H₄]

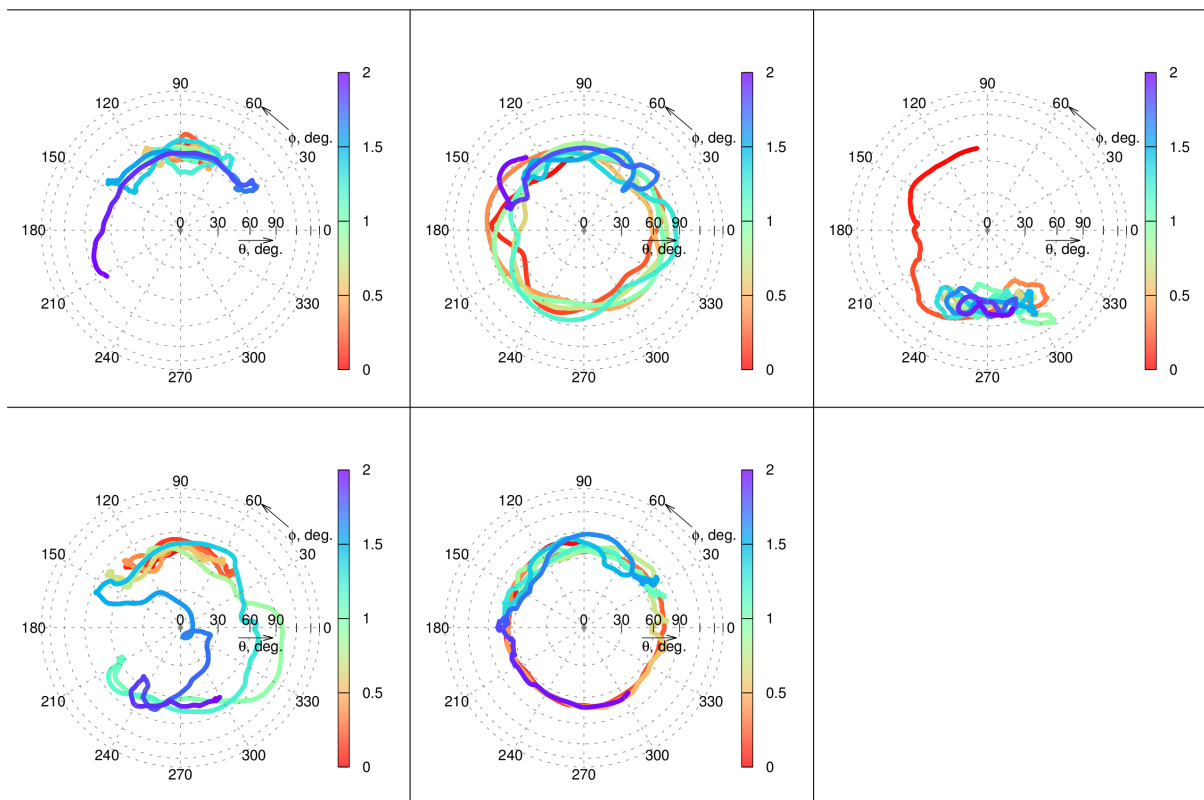
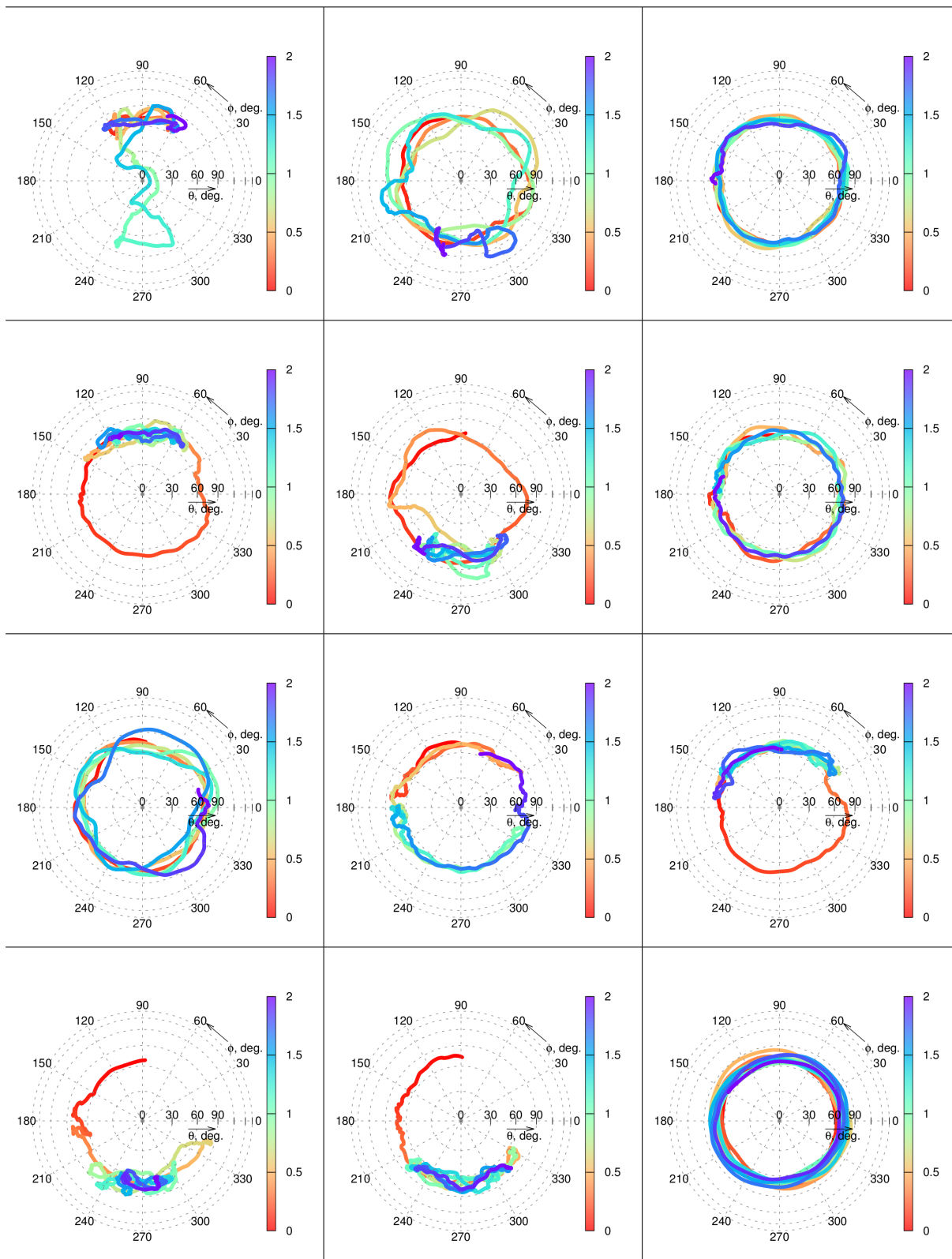
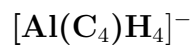
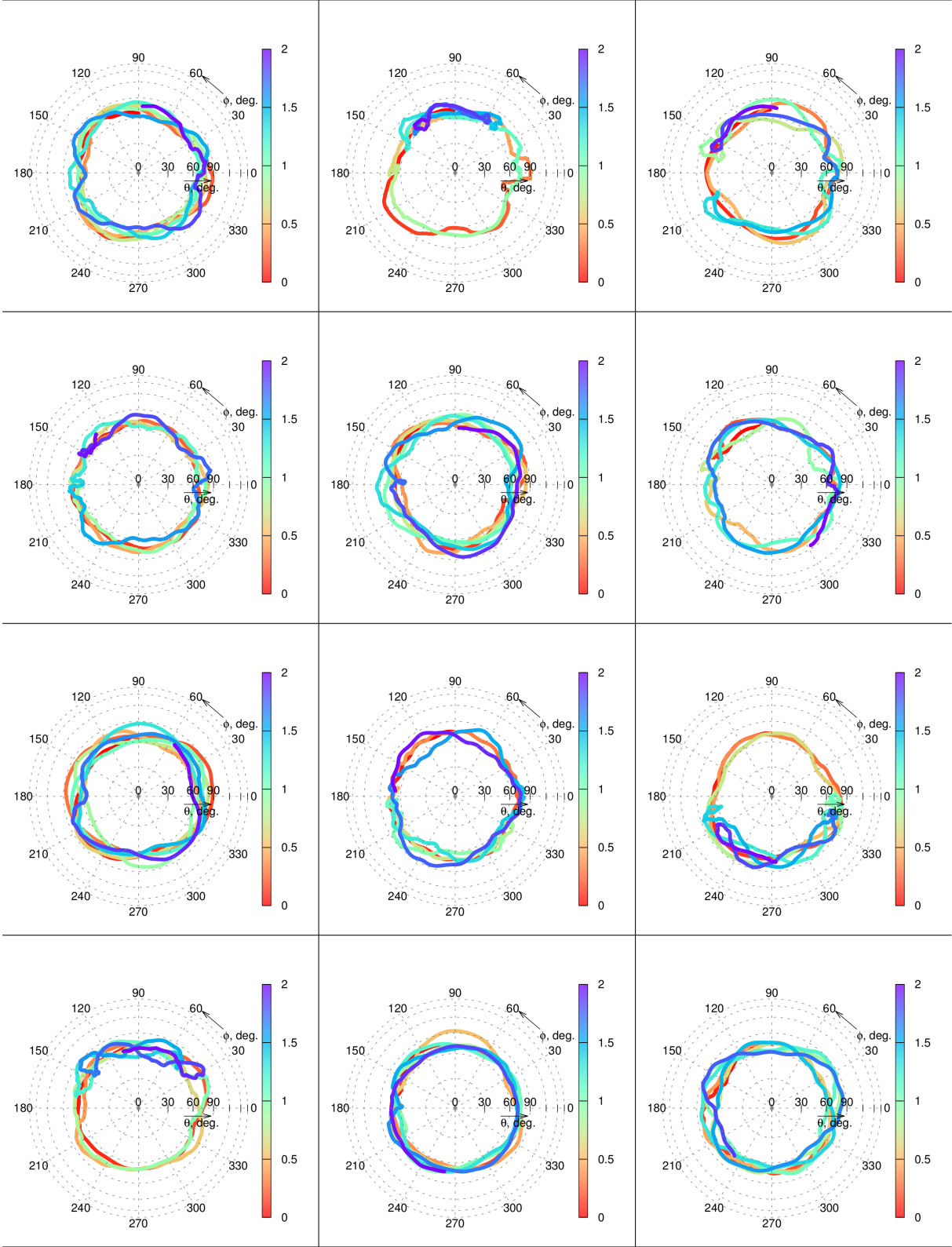


Figure S3: Reactive 5 trajectories for the Si system. Time evolution (2 ps) of internal coordinates: angle between two three-membered rings (ϕ , degree), and $\angle X-C1-C2$ (θ , degree). Color coded as (0→2 ps corresponding red→blue).





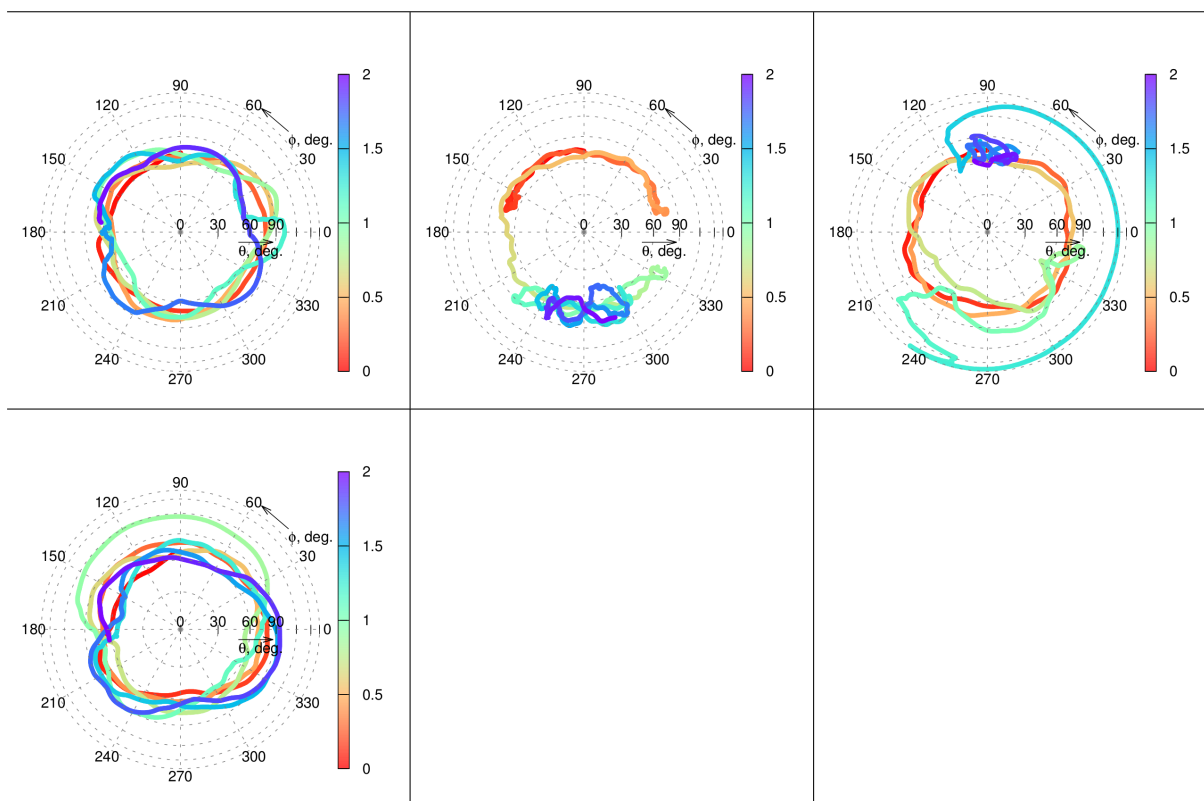
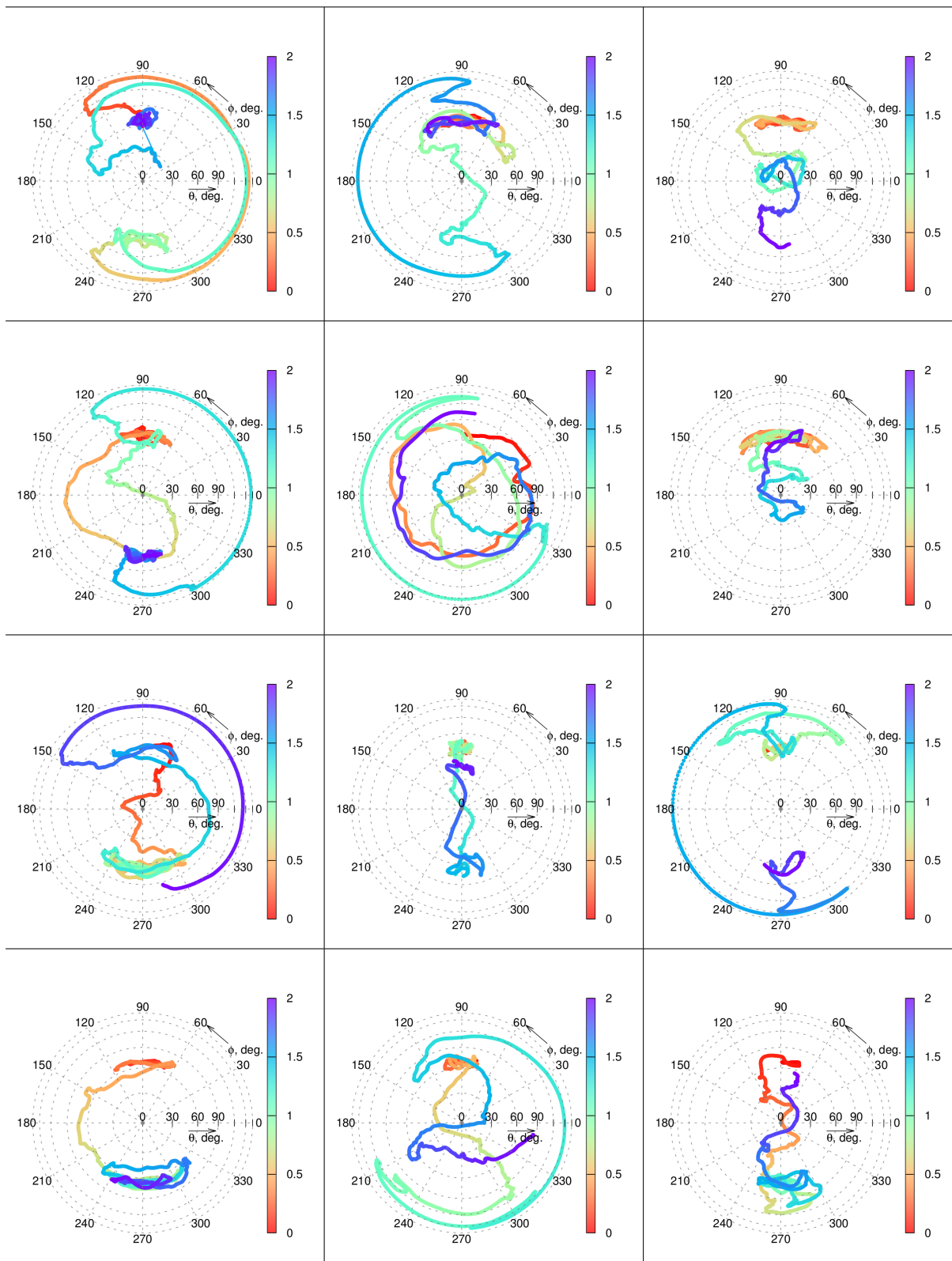
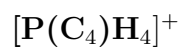
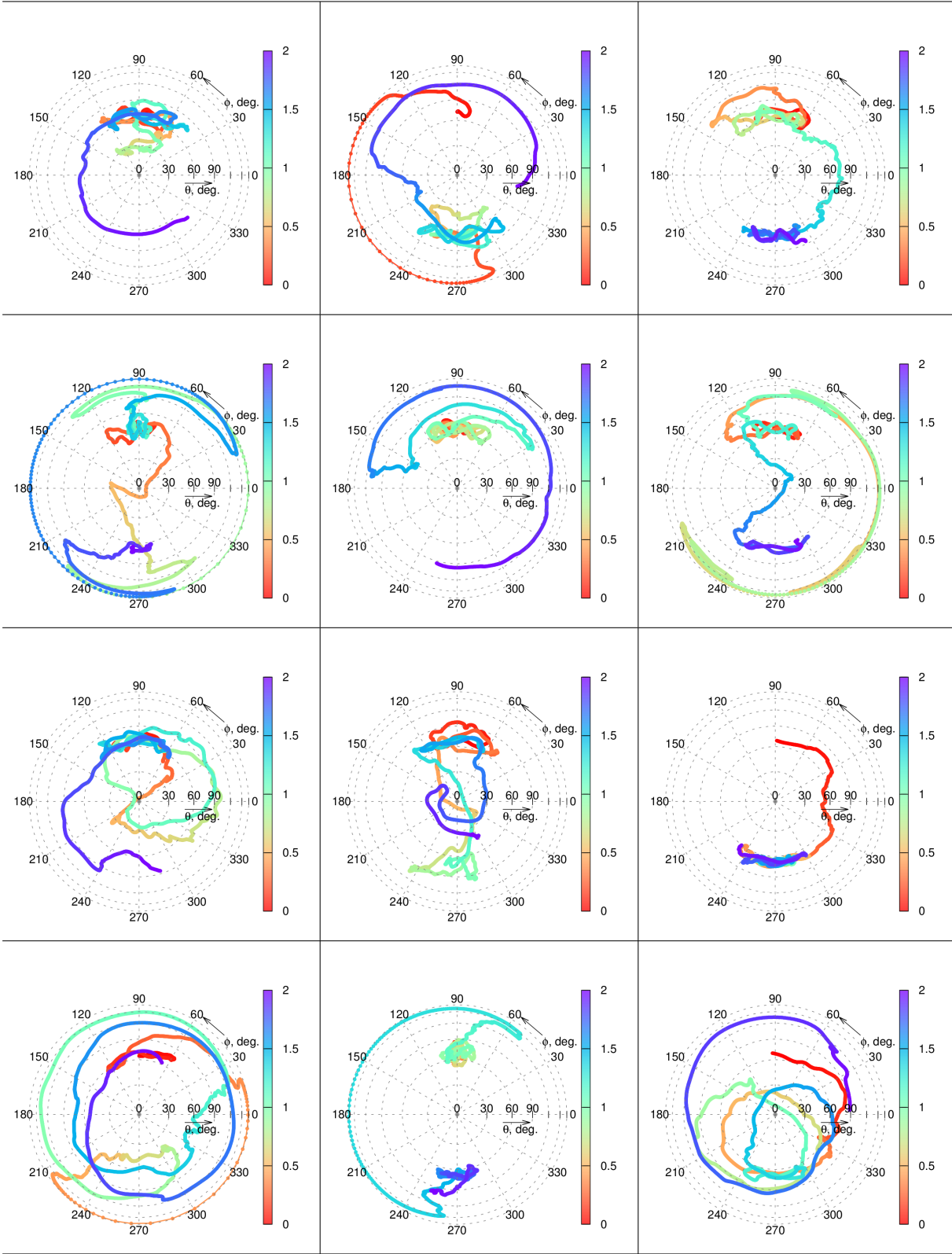


Figure S4: Reactive 28 trajectories for the Al^- system. Time evolution (2 ps) of internal coordinates: angle between two three-membered rings (ϕ , degree), and $\angle\text{X-C1-C2}$ (θ , degree). Color coded as (0→2 ps corresponding red→blue).





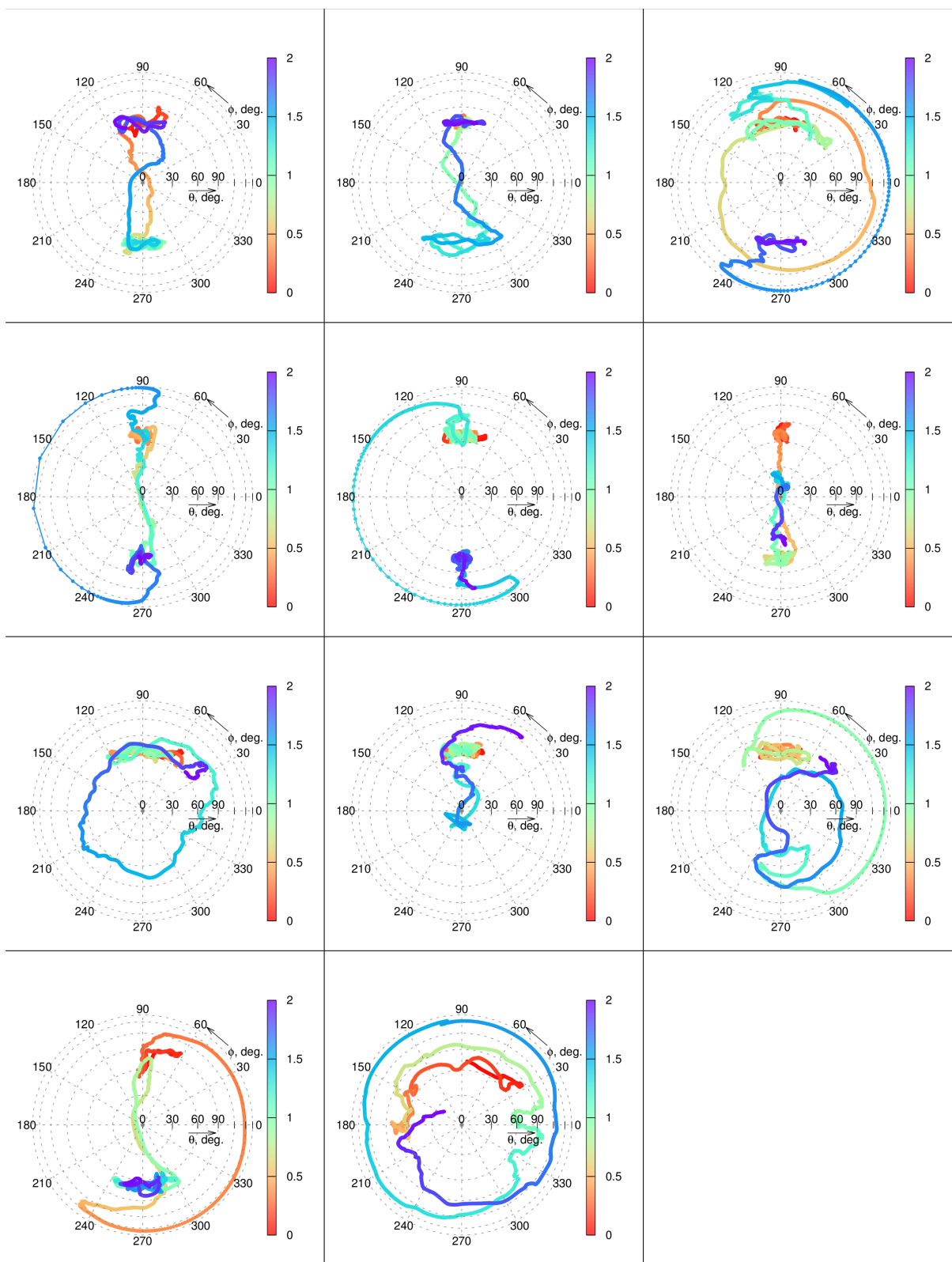


Figure S5: Reactive 35 trajectories for the P^+ system. Time evolution (2 ps) of internal coordinates: angle between two three-membered rings (ϕ , degree), and $\angle X-C1-C2$ (θ , degree). Color coded as (0→2 ps corresponding red→blue).

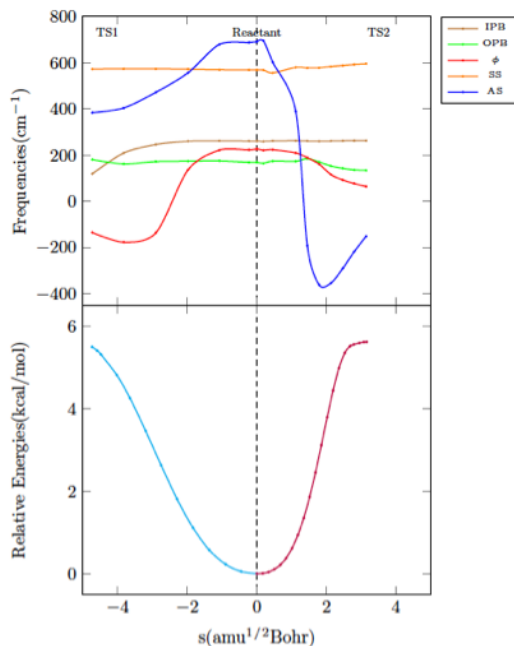


Figure S6: Comparison of harmonic vibrational frequencies along IRC paths for the $[\text{P}(\text{C}_4)\text{H}_4]^+$ molecule. P–C symmetric stretch and asymmetric stretch; torsional and bending vibrations.

The variation of the frequency of the asymmetric P–C stretch along the dissociative reaction path is much larger compared to that of the variation seen for the torsional frequency. In addition, the P–C stretching frequency falls with the range of the torsional frequency in certain region of IRC. Thus the possibility of efficient intramolecular vibrational energy redistribution (IVR) between the asymmetric P–C stretch and the low frequency torsional and bending vibrations along the dissociative reaction path can be seen leading to more trajectories following the dissociative reaction pathway. In the case of the nondissociative isomerization, the coupling between the low frequency and the P–C stretching modes are absent thus facilitating localization of the energies in torsional modes.

Lifetime for isomerization from the trajectories The lifetime from each trajectory undergoing stereomutation were calculated following the angle between the planes (ϕ) and $\angle\text{X-C1-C2}$ (θ) as a function of time. Only the first event of stereomutation was considered in calculating the lifetimes. The transition state structures for stereomutation for $\text{X} = \text{Si}$ and Al^- are planar ($\phi = 0^\circ$). Thus, the lifetime is defined as the time taken by the trajectory

when ϕ changes sign (planar geometry) and θ takes a value between θ_1 and θ_2 . The critical values of θ_1 and θ_2 corresponding to the dissociative transition states are given in Table S6. All the 28 and 5 trajectories undergoing stereomutation for $X = \text{Al}^-$ and Si, respectively did not show any ring opening process prior to the first event of stereomutation. Finally, the lifetimes determined from each trajectory was averaged to obtain the average lifetime of the isomerization process. However, for $X = \text{P}^+$, the transition state structures are non-planar with $\phi = 31.5^\circ$ and -31.5° . The two degenerate transition states are connected via a planar intermediate leading to a double well potential. In this scenario, the stereomutation occurs when the the molecule crosses the second barrier (TS1'), i.e., when $\phi < -31.5^\circ$. Hence the lifetime was calculated when the trajectory crosses the clockwise ($\phi = -31.5^\circ$) or anti-clockwise transition states ($\phi = -148.5^\circ$). It was found that of the 8 trajectories showing stereomutation, 4 were recrossing the TS2 (ring opening transition state) before undergoing stereomutation. Such recrossing trajectories were not taken into account while calculating the average lifetimes. Similar procedure was used for the calculation of lifetimes in the case of $[\text{Si}(\text{C}_2\text{NB})\text{H}_2(\text{CH}_3)_2]$.

Table S6: θ and ϕ parameters used for the calculation of lifetimes for various systems.

Systems	θ for ring opening TS ($^\circ$)		ϕ for stereomutation ($^\circ$)	
	θ_1	θ_2	Clockwise	Anticlockwise
$[\text{Si}(\text{C}_4)\text{H}_4]$	14.6	154.3	0.0	180.0
$[\text{Al}(\text{C}_4)\text{H}_4]^-$	25.2	137.8	0.0	180.0
$[\text{P}(\text{C}_4)\text{H}_4]^+$	49.5	92.8	-31.5	-148.5
$[\text{Si}(\text{C}_2\text{NB})\text{H}_2(\text{CH}_3)_2]$ (Si-B bond breaking)	17.2	148.3	-23.0	-164.1

Rice-Ramsperger-Kassel-Marcus (RRKM) Lifetimes The RRKM^[6-9] rate constants were computed for all the four model systems using the expression,

$$k(E) = \frac{G(E - E^\ddagger)}{h \rho(E)} \quad (2)$$

where $G(E - E^\ddagger)$ is the sum of states at the transition state region, $\rho(E)$ is the density of states at the minima, E^\ddagger is the barrier for the reaction, and E is the total energy above the classical minima. The rate constants were computed with the total energy used in the trajectory simulation. The density and sum of states were computed by classical counting at a rotational temperature of 0 K. Since for $X = \text{Si}$, Al^- , and P^+ , the systems are symmetric, so the stereomutation via clockwise and anticlockwise rotation are degenerate and hence a factor of two was used for the reaction path degeneracy.

However, the stereomutation for $X = \text{P}^+$ and $[\text{Si}(\text{C}_2\text{NB})\text{H}_2(\text{CH}_3)_2]$ spiro systems is a two-step process with rate constants k_1 and k_2 : (1) $\text{R} \rightarrow \text{Int1}$ (k_1) and (2) $\text{Int1} \rightarrow \text{R}'$ (k_2); the overall rate constant for these systems is given by the expression $K = k_1/2$.

The lifetimes were then computed from the RRKM rate constant values obtained ($\tau = 1/K$). The lifetimes of all the four systems were found to be in picosecond timescales.

We have also performed a TST rate constant calculation that includes tunnelling coefficient $C(T)$ that uses a one-dimensional Eckart barrier. We found that $C(T)$ was only 1.01, i.e., about 1% at 300 K.

4. Dynamics using BOMD simulations

A continuous part of the BOMD trajectory exhibiting the transitions between **t-Si** and **t*-Si** via either **p-Si** or **p*-Si** transition states is used to make a movie. The traversing of the molecule as observed in the BOMD simulation is captured on the $E(\theta, \phi)$ surface (The two identical carbond atoms C1 and C2 are colored differently for clarity). See attached file (r_to_s_transition.mp4).

4.1 Kinetic analysis by MSM

We have used following geometric criteria for clustering conformations (**t**, **t***, **r** and **r*** four representative states depicted in Figure 2(a), main text) from BOMD simulations of the $\text{Si}(\text{C})_4\text{H}_4$ molecule:

$$\mathbf{t} : r_{\text{Si-C1}} \leq 2.5, r_{\text{Si-C2}} \leq 2.5, 0^\circ \leq \phi \leq 180^\circ$$

$$\mathbf{t}^* : r_{\text{Si-C1}} \leq 2.5, r_{\text{Si-C2}} \leq 2.5, -180^\circ \leq \phi \leq 0^\circ$$

$$\mathbf{r} : r_{\text{Si-C1}} \leq 2.5, r_{\text{Si-C2}} \geq 2.5, -180^\circ \leq \phi \leq 180^\circ$$

$$\mathbf{r}^* : r_{\text{Si-C1}} \geq 2.5, r_{\text{Si-C2}} \leq 2.5, -180^\circ \leq \phi \leq 180^\circ$$

Bond distances are in Å, and ϕ refers to the angle between two three-membered rings of the spiro- $\text{Si}(\text{C})_4$ motif. We have used 661160 number of conformations from a 400 ps long trajectory with the step-size of $0.0242 \times 25 \text{ fs} = 0.605 \text{ fs}$ (0.000605 ps).

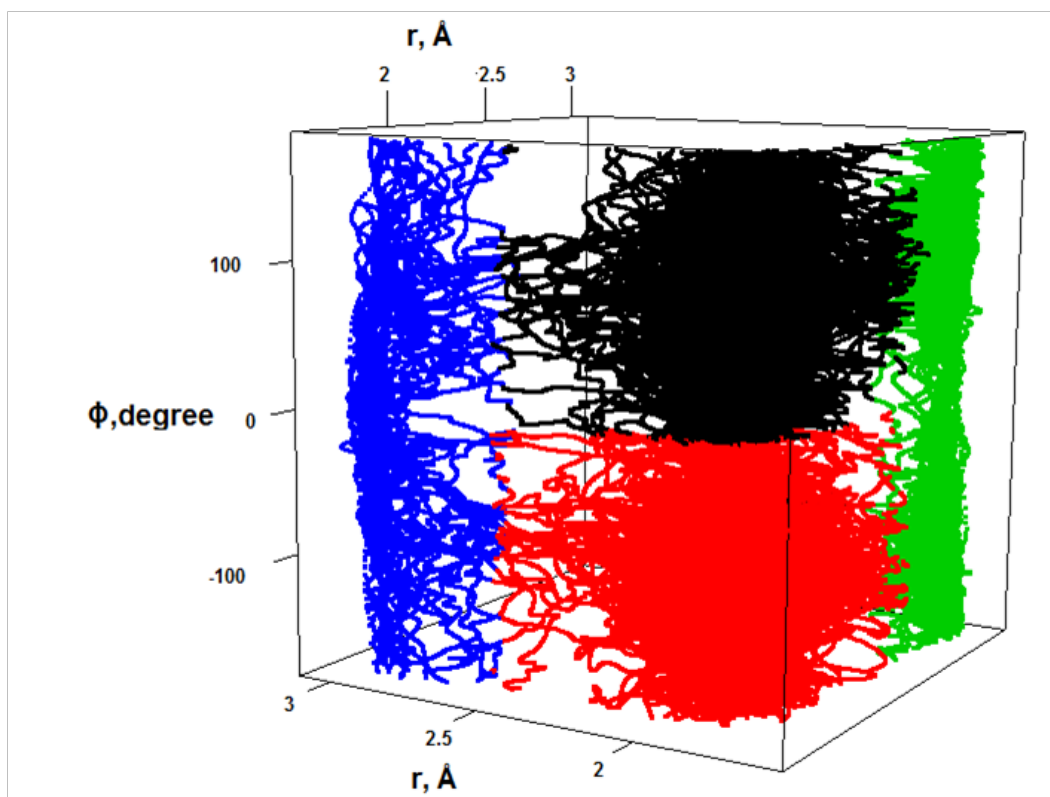


Figure S7: Conformational clustering of four states.

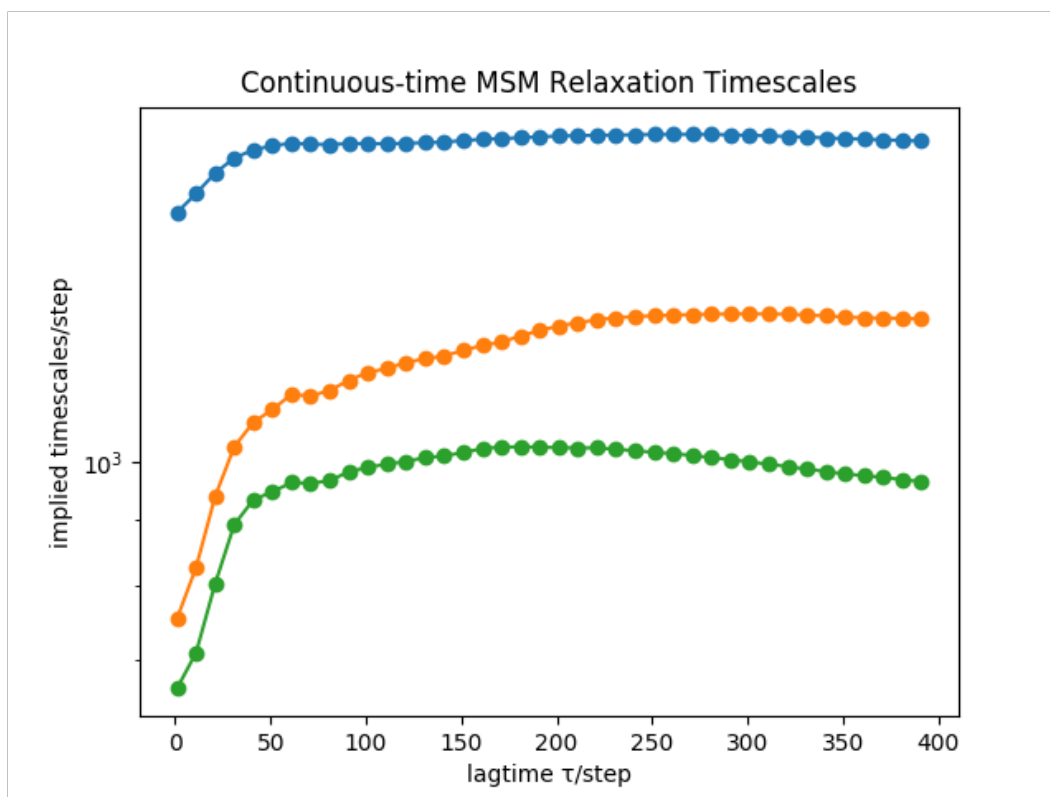


Figure S8: Implied time scale vs. Lag time, step.

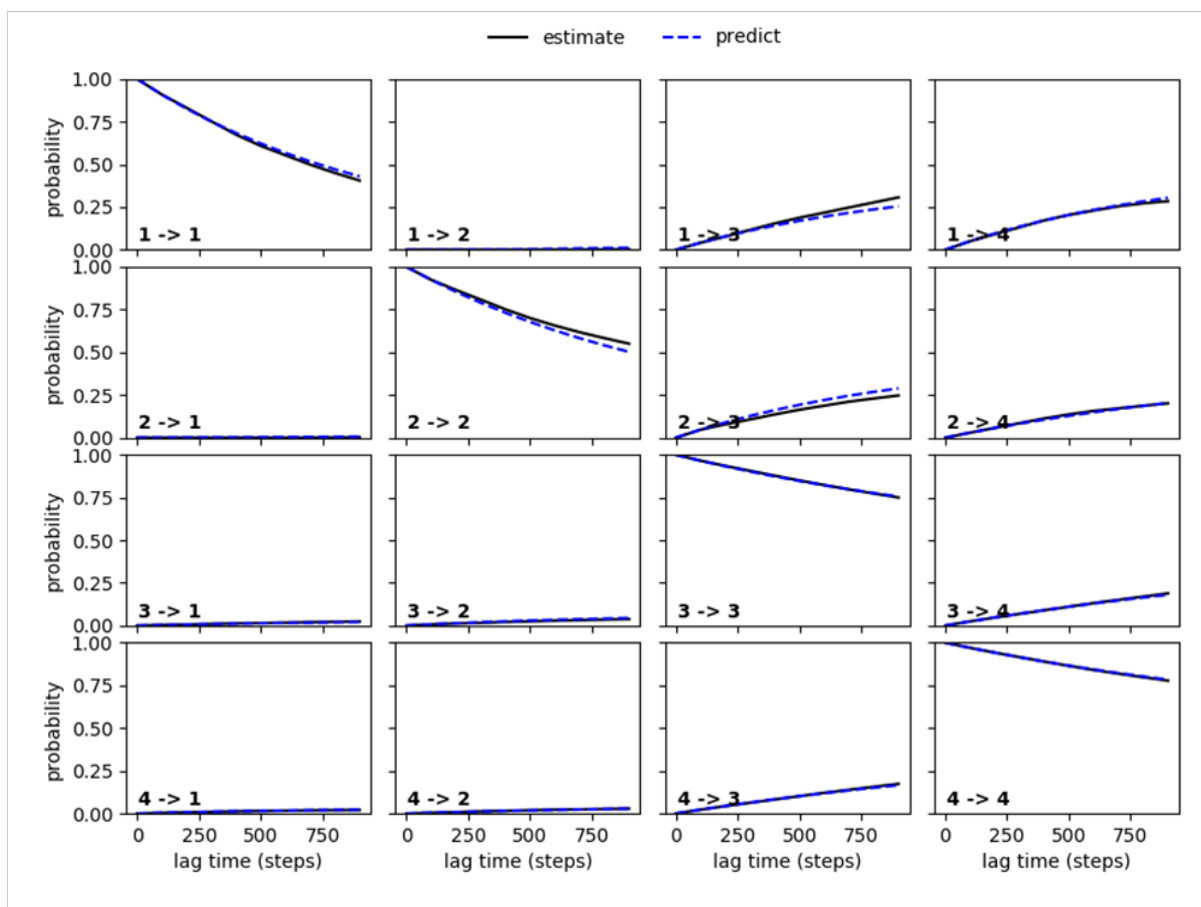


Figure S9: Transition probabilities predicted by the MSM parameterized at lag time $\mathcal{L}=100$ steps (0.06 ps)

4.2 Lifetime of closed and open states

Dwell time distributions $P(t; t_d^*)$ of closed and open states were obtained from a 400 ps long BOMD trajectory of the $\text{Si}(\text{C})_4\text{H}_4$ molecule at $t_d^* = 0.005$ ps. Survival probability distributions $S(t; t_d^*)$ were then calculated using dwell time distributions followed by the best fit to a triexponential function, by which the average lifetimes (Figure 4(c) in main text) of closed and open states were calculated.

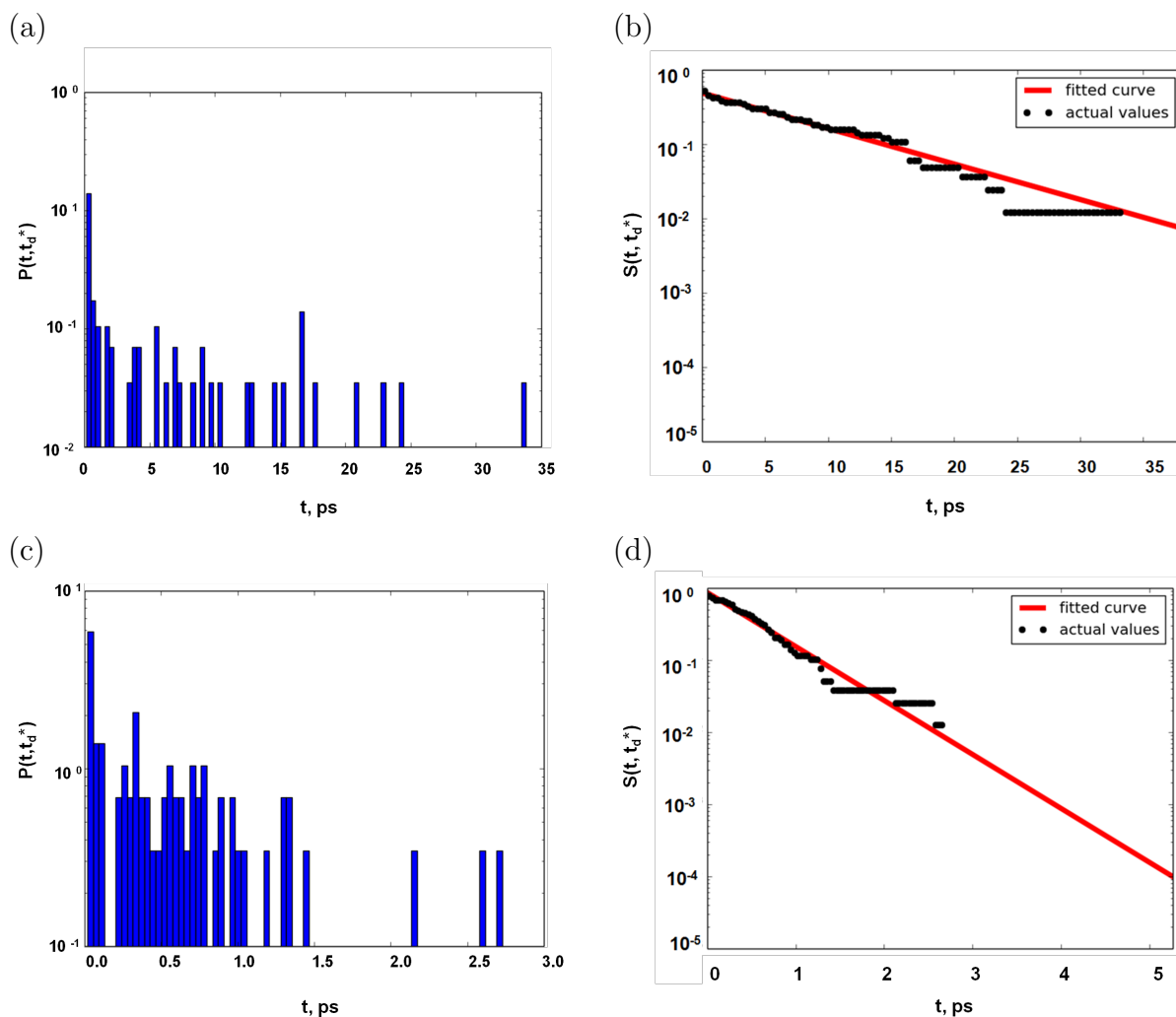


Figure S10: Lifetime calculations of closed (t and t^*) and open (r and r^*) states at $t_d^* = 0.005$ ps. Dwell time distributions $P(t; t_d^*)$ for closed (a) and open (b) states. Survival probability distributions $S(t; t_d^*)$ shown in black dots, and the best fit triexponential function for $S(t; t_d^*)$ indicated by red line for closed (b) and open (c) states.

5. Structures, energies and dynamics of chiral-Si system

In case of the chiral-Si system, structures and energetics were obtained at the MP2/cc-pVTZ level of theory. Ab initio classical trajectories were computed at the MP2/6-31+G(d) level.

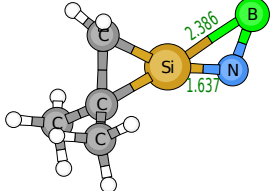
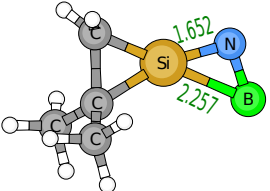
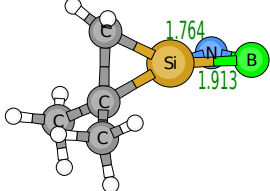
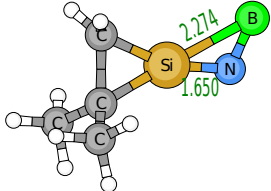
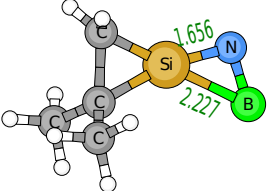
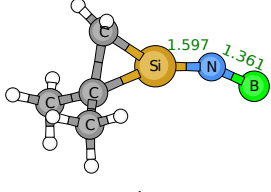
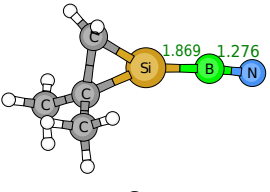
[Si(C ₂ NB)H ₂ (CH ₃) ₂], intermediates		
		
Z $\theta = 104.9^\circ$ $\phi = 0.0^\circ$ $N_{imag} = 0$	E $\theta = 96.5^\circ$ $\phi = 180.0^\circ$ $N_{imag} = 0$	R/S $\theta = 75.3^\circ$ $\phi = 90.0^\circ$ $N_{imag} = 0$
[Si(C ₂ NB)H ₂ (CH ₃) ₂], transition states		
		
ts1 $\theta = 97.7^\circ$ $\phi = 21.3^\circ$ $N_{imag} = 1(101.9i)$	ts2 $\theta = 94.8^\circ$ $\phi = 10.1^\circ$ $N_{imag} = 1(53.8i)$	
[Si(C ₂ NB)H ₂ (CH ₃) ₂], ring-opened states		
		
r1 $\theta = 158.6^\circ$ $\phi = 0.0^\circ$ $N_{imag} = 2(66.9i, 32.3i)$	r2 $\theta^a = 175.5^\circ$ $\phi = 0.0^\circ$ $N_{imag} = 0$	
Species	E_{rel}	
Z	8.016	
E	6.976	
R/S	0.00	
ts1	8.124	
ts2	6.984	
r1	9.922	
r2	22.626	

Figure S11: Optimized structures and selected geometrical parameters of two planar (p1 & p2), tetrahedral (t) minima, and two transition states (ts1 & ts2) of the chiral-Si system at MP2/cc-pVTZ level of theory. Bond distances (in Å), angle between two three-membered rings (ϕ , degree), \angle Si-N-B (θ , degree), and N_{imag} representing number of imaginary frequency with values given in parentheses. Relative energies of transition states/intermediates (in kcal mol⁻¹) at the MP2/cc-pVTZ level of theory for the chiral-Si system. ^a \angle Si-B-N

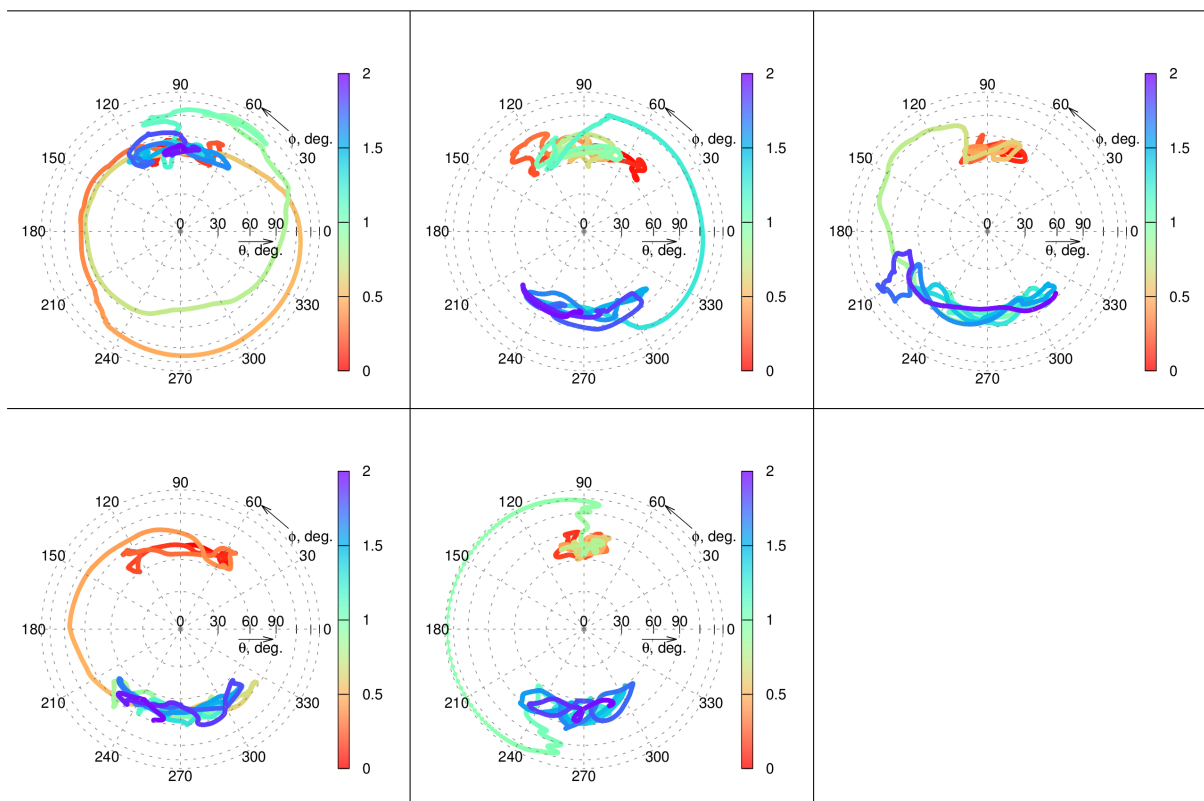


Figure S12: Reactive 5 trajectories for the chiral-Si system. Time evolution (2 ps) of internal coordinates: angle between two three-membered rings (ϕ , degree), and $\angle\text{Si-N-B}$ (θ , degree). Color coded as (0 \rightarrow 2 ps corresponding red \rightarrow blue).

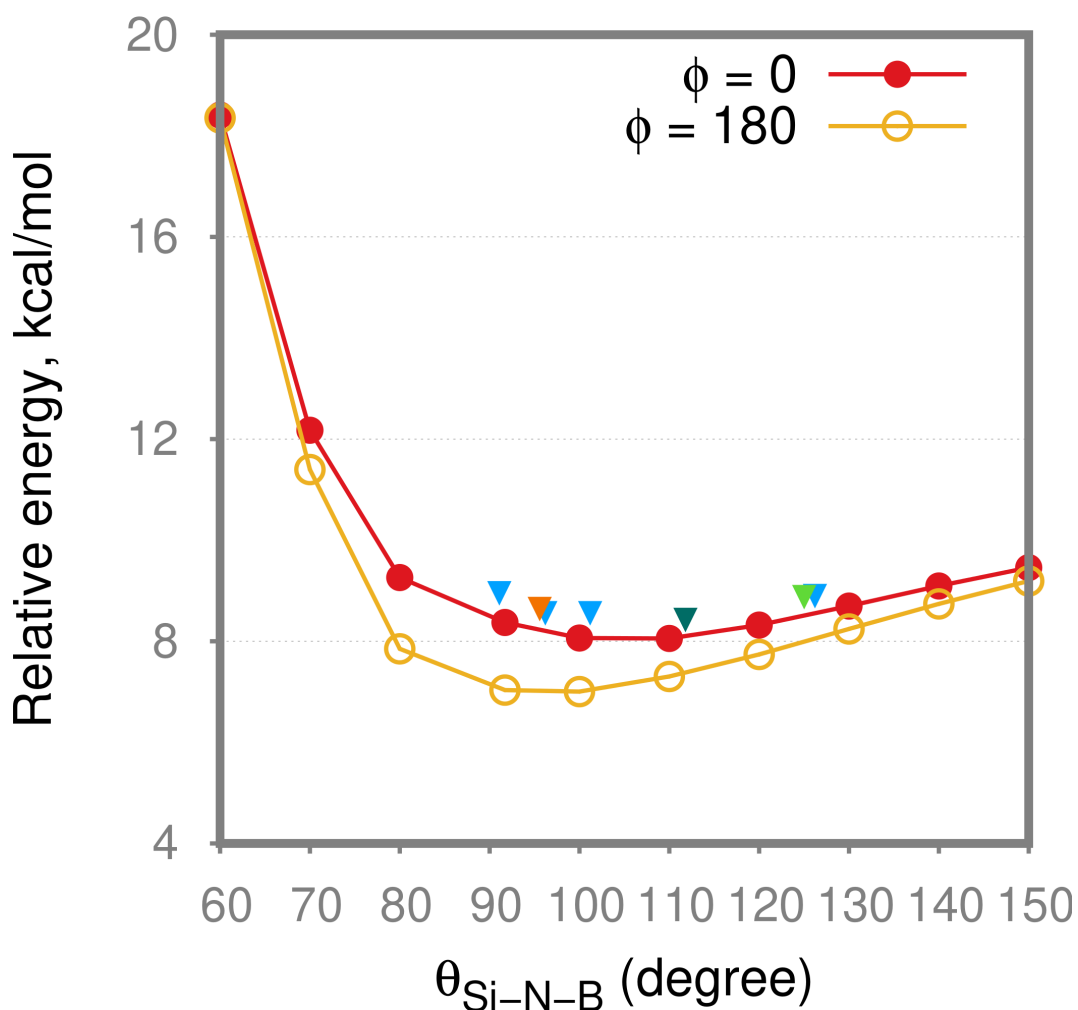


Figure S13: PESs of the (Z) and (E) ($\phi = 0$ and 180 degree respectively) states of the chiral system (in kcal mol⁻¹) with respect to $\angle\text{Si-N-B}$ (θ , degree) obtained at the MP2/cc-pVTZ level of theory. Five reactive trajectories (see Fig. S12), except the last one consist of seven racemization events. The values of θ of the planar states in the trajectory during the process of racemization are marked by inverted triangles. Based on the fact that these points lie in the shallow potential energy minimum as that of the planar state, they were considered to be closed state.

REFERENCES

- (1) Hopffgarten, M. v.; Frenking, G. Energy decomposition analysis. *Wiley Interdisciplinary Reviews: Computational Molecular Science* **2012**, *2*, 43–62.
- (2) Snijders, J.; Vernooijs, P.; Baerends, E. Roothaan-Hartree-Fock-Slater atomic wave functions: single-zeta, double-zeta, and extended Slater-type basis sets for $_{87}\text{Fr}$ - $_{103}\text{Lr}$. *Atomic Data and Nuclear Data Tables* **1981**, *26*, 483–509.
- (3) te Velde, G.; Bickelhaupt, F. M.; Baerends, E. J.; Fonseca Guerra, C.; van Gisbergen, S. J. A.; Snijders, J. G.; Ziegler, T. Chemistry with ADF. *J. Comput. Chem.* **2001**, *22*, 931–967.
- (4) Guerra, C. F.; Snijders, J.; te Velde, G. t.; Baerends, E. Towards an order-N DFT method. *Theor. Chem. Acc.* **1998**, *99*, 391–403.
- (5) Baerends, E. J. et al. ADF2017, SCM, Theoretical Chemistry, Vrije Universiteit, Amsterdam, The Netherlands, <https://www.scm.com>.
- (6) Marcus, R. A.; Rice, O. The kinetics of the recombination of methyl radicals and iodine atoms. *J. Chem. Phys.* **1951**, *55*, 894–908.
- (7) Marcus, R. A. Unimolecular dissociations and free radical recombination reactions. *J. Chem. Phys.* **1952**, *20*, 359–364.
- (8) Rosenstock, H. M.; Wallenstein, M.; Wahrhaftig, A.; Eyring, H. Absolute rate theory for isolated systems and the mass spectra of polyatomic molecules. *Proc. Natl. Acad. Sci. USA* **1952**, *38*, 667.
- (9) Zhu, L.; Hase, W. L. A general RRKM program. QCPE 644, Quantum Chemistry Program Exchange, Indiana University.

pccp_si.pdf (7.67 MiB)

[view on ChemRxiv](#) • [download file](#)

Other files

out5a-1.mp4 (7.07 MiB)

[view on ChemRxiv](#) • [download file](#)
